LONG-PERIOD GRATINGS AS IMMUNO-DIAGNOSTIC BIOSENSORS

by

Tiffanie Gabrielle D'Alberto

thesis submitted to the faculty of the

Virginia Polytechnic Institute & State University

in partial fulfillment of the requirements for the degree of

Master of Science in Electrical Engineering

_____

Dr. K. Murphy, Chair

_____ _____

Dr. R. Claus **Dr. I. Besieris**

January, 1997

Blacksburg, Virginia

Dedicated to my family
and in loving memory of my Topaz.

To my knowledge,
no animals were sacrificed for this research.

ABSTRACT

This research presents a novel biosensor which utilizes the refractive index sensitivity of a fiber optic long-period grating. The long period grating couples light from the forward propagating guided core mode of a single-mode fiber into discrete circularly symmetric cladding modes. Due to imperfections in the cladding surface, loss bands are seen in the transmission spectrum corresponding to the coupled wavelengths. Based on the phase-matching condition between the coupling and coupled modes, the loss bands shift with changes in the refractive index of the surrounding medium. The grating surface is chemically treated to covalently bond antibody to the cladding of the sensor. Treatment with the proper antigen increases the effective index seen by the cladding modes and affects the placement of the loss bands. This sensor demonstrates specific antigen binding capacity with loss band shifts of 10 nm or more. The device offers several advantages over the widely used Enzyme-Linked Immuno-Sorbent Assays. Diagnostic applications can be expanded beyond the tests presented here.

TABLE OF CONTENTS

LIST OF FIGURES

LIST OF TABLES

1.0 INTRODUCTION

One of the many interesting applications of electromagnetics is found in the field of biosensors. Much research has gone into the study of antigen detection, drug recognition, and the development of antibodies in order to diagnose and treat harmful illnesses. Previous to the last decade or so, most biological reactions have been monitored predominantly on a chemical basis. The Enzyme-Linked Immuno-Sorbent Assay (ELISA) is a good example. The assay allows researchers to assess whether or not a reaction is taking place and to what degree [1]. Though the ELISA is the chief means of antibody-antigen interaction detection today, it has the drawbacks of requiring chemical treatment of the measurand and several time-consuming steps [2]. Constructing a more desirable means of detection to yield real-time results with a minimum of preparation techniques is the motivation behind attempting to use long-period gratings as fiber optic biosensors. By incorporating electromagnetics into immunoassays, sensitive, real-time, convenient sensors have been achieved.

Chapter 2 offers an understanding of the fundamentals of the involved biochemistry. Antigen-antibody interactions are explained as they relate to the field of immunoassays. Several assays which are in use today are discussed and critiqued. Chapter 3 discusses the long-period grating. Wave propagation plots (β-plots) and wavelength versus grating period curves (λ vs Λ curves) are detailed to model sensor operation. Refractive index sensing is explored, and temperature and strain cross-sensitivity are addressed. Chapter 4 considers implementation of the sensor, from fabrication of the long-period grating to coating the glass surface for antibody attachment. Chapter 5 goes through the experimental results and procedures of what did and did not meet with success. Chapter 6 concludes this thesis with some ideas for future research.

2.0 BIOCHEMICAL BACKGROUND

This chapter offers a description of antibodies and antigens. Specific properties of antibodies as they relate to this thesis are explored. Several common types of immunoassays, both chemical and optical, are compared and critiqued.

2.1 ANTIBODIES AND ANTIGENS

Antibodies are the complex compounds which organisms produce to fight off foreign substances which invade the body. Antigens are the chemically reactive units unrecognized by the body's immune system which are subject to an antibody attack. The antibody attaches itself to reactive portions of the antigen through the antibody's active sites. Binding renders the antigen inert by destroying the compound, sterically hindering its reactive segments, or rendering such segments inactive through direct attachment.

As Figure 1 shows, all antibodies are made from the same basic unit consisting of four polypeptide sequences bound by di-sulfide and covalent bonds [1]. The four sequences are grouped into pairs: the light chains and the heavy chains [1]. At the top of the unit are two active sites encompassing portions of both chains [1]. It is these active sites which are integral to the antigen-antibody interaction.

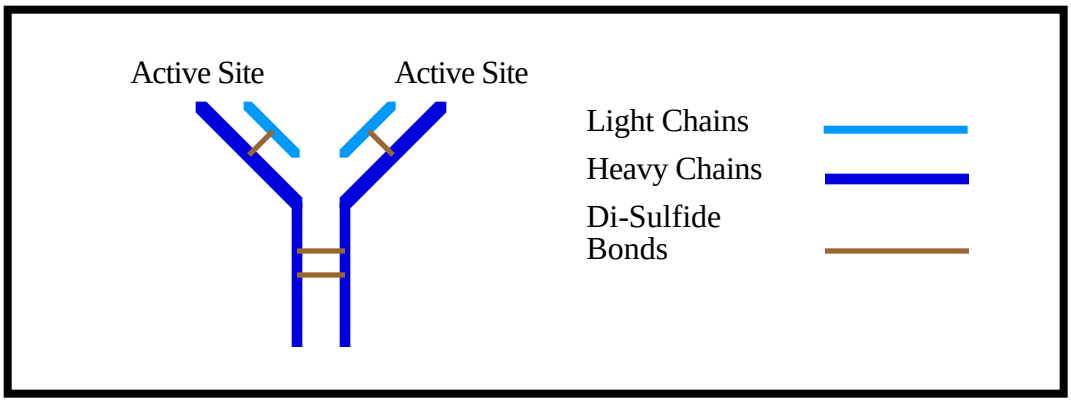

Figure 1: Basic structural unit of the antibody. [1]

The basic unit of the antibody can also be described by its components upon pepsin or papain cleavage, as demonstrated in Figure 2 [1]. Pepsin cleavage separates the antibody between the two main di-sulfide bonds of the heavy chains [1]. The two resulting portions are the $F(ab')_2$ fragment containing the active sites and Fc fragment containing classification information [1]. Upon papain cleavage, the antibody is split into three portions preserving the double di-sulfide bond in the heavy chains [1]. The result is an Fc fragment and two Fab fragments [1]. Cleaving the antibody has importance in isolating the active sites within the $F(ab')_2$ or Fab fragments and characterizing the class of antibody based on its Fc fragment.

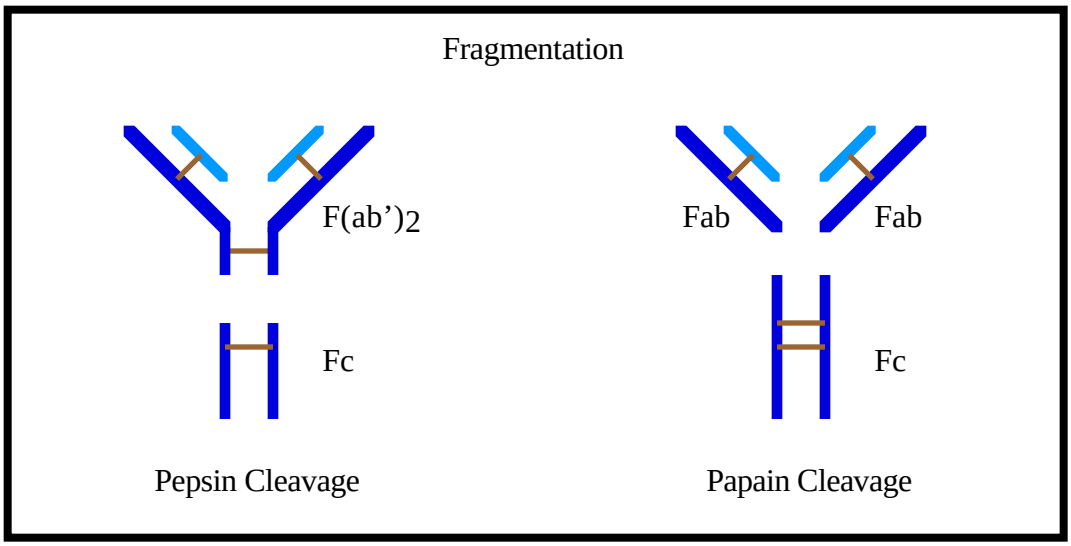

Figure 2: Pepsin and papain cleavage to characterize antibody fragments. [1]

There are five classes of antibody (immunoglobulin or Ig) produced by mammals [1]. Part of the classification is rooted in how many basic units make up the individual antibody [1]. A monomer has one basic unit, a dimer two, etc.. The main foundation for classification, however, is the chemical composition of the Fc fragment. The heavy chains of the antibody have designations γ, α, μ, ε, and δ which gives rise to their classification names: IgG, IgA, IgM, IgE, and IgD [1]. Figure 3 gives the fundamental structures and characteristics associated with each class of antibody. IgG is the class predominantly produced in mammals, and therefore the one which is most often used in research [1].

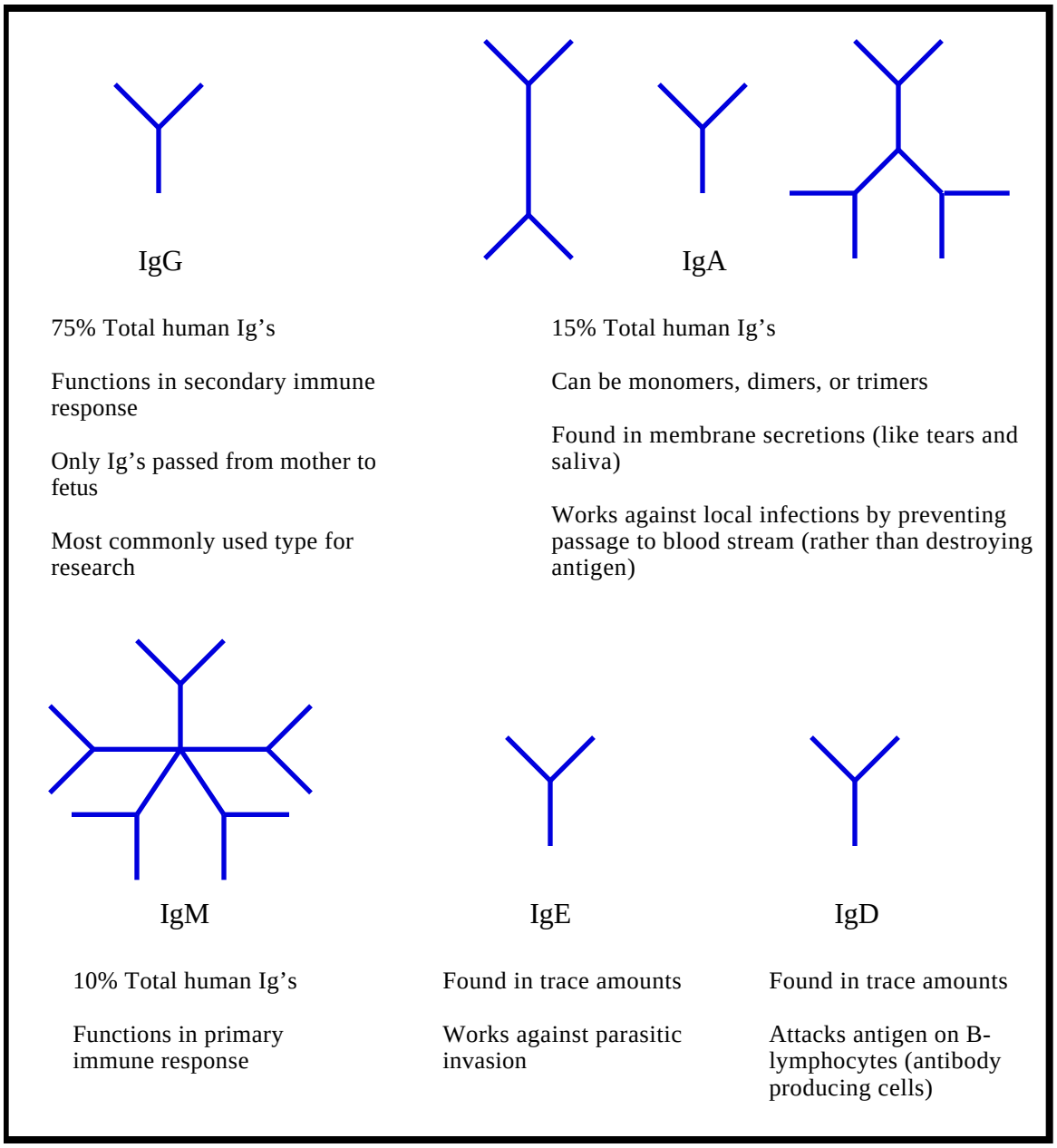

Figure 3: The five main classes of antibody (immunoglobulin). [1]

B-lymphocytes are the cells responsible for antibody production [1]. Each cell can produce one class of immunoglobulin with one pair of active sites [1]. The term monoclonal antibodies refers to antibodies derived from a single cell type which can bond to only one or two specific functional groups. An antigen, however, has many different functional groups which need to be hindered before the antigen becomes inert [1]. As a result, a grouping of cells producing different

antibodies with distinct binding capacities is needed [1]. Antibodies created by a group of cells targeting the same antigen are referred to as polyclonal [1]. A representation of this is given in Figure 4.

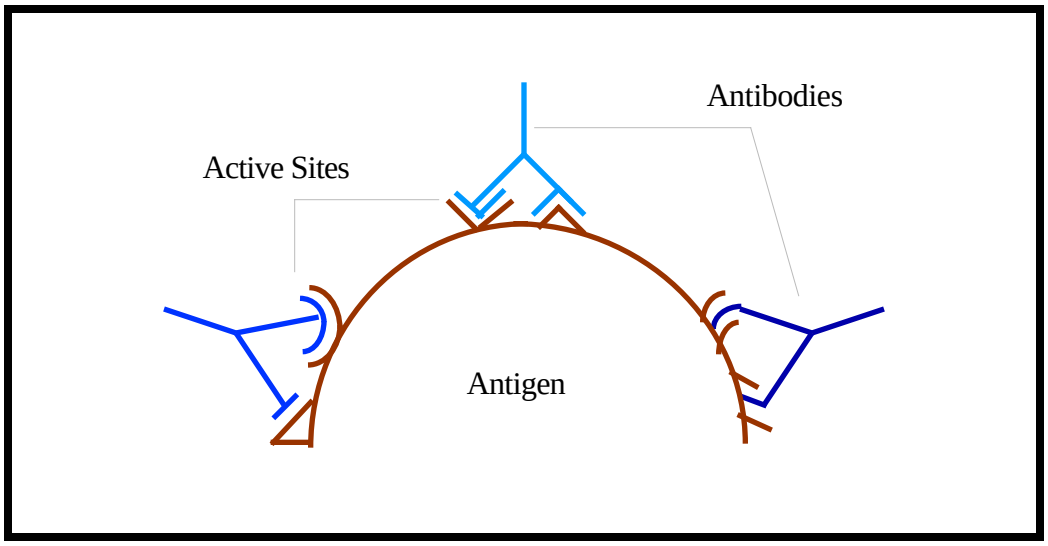

Figure 4: Representation of three monoclonal IgG's working as a group of polyclonal antibodies against reactive portions of an antigen.

2.2 THE IMMUNOASSAY

This section outlines the basic principles behind immunoassays. Specific assays are outlined including the Enzyme-Linked Immuno-Sorbent Assay, surface plasmon resonance, and the tapered fiber sensor.

2.2.1 MAJOR CONSIDERATIONS

There are three main concerns in an immunoassay. One, the antibody has to be immobilized. The antigen-antibody interaction must occur in some localized area in order to be detected. During a test, the sensing apparatus may undergo washing or other stressful handling techniques to remove excess chemicals [3]. The antibody needs to remain intact during these procedures. Good

adhesion is usually accomplished by coupling to a substrate through adsorption or covalent binding, the latter being the most effective. Adsorption involves weak bonds (hydrogen, Van der Waals) between various portions of the antibody and the substrate. Plastic polymers work well for this type of immobilization [3]. Covalent bonding requires the substrate to react with very specific functional groups on the antibody, in this way allowing the investigator the freedom to choose what portion of the antibody is left to react with the antigen [4]. Covalent bonding allows the active sites to remain unobstructed and chemically reactive [4].

Two, the active sites of the antibody must be preserved to ensure the antigen of interest will be bound efficiently. Several factors can inhibit, denature, or impede an active site. Temperature, pH, and caustic chemicals have to be carefully monitored [1]. The orientation of the antibody with respect to the substrate must be considered to allow enough room for the antigen-antibody interaction. Also, special care must be taken to ensure that no chemical in the assay binds to the active site of the antibody more readily than would the antigen. The use of $F(ab')_2$ and Fab fragments in lieu of whole immunoglobulins can aid in the preservation of active sites at the cost of time-consuming or expensive cleavage [5].

Third, the antigen must react with the antibody. Reactions with the sensing apparatus can occur and must be avoided [3]. To do so, blocking agents are used to ensure that the antigen can only react in predictable ways [4]. For instance, if an antibody is absorbed onto a plastic polymer, it is likely that parts of the substrate will remain uncovered [3]. If an antigen is introduced into this environment, it could fill the empty spaces without direct antibody interaction, thus giving a false positive test [3]. Blocking agents such as bovine serum albumen are designed to react quickly with almost any substrate, thus ensuring that antigen binding can occur only through specific immunoglobulins [4].

2.2.2 THE SANDWICH ELISA

Currently, the most widely used immunoassay for rapid qualitative and quantitative assessment of antigen-antibody interactions is the ELISA, Enzyme-Linked Immuno-Sorbent Assay [2]. ELISA is

antigen-antibody interactions is the ELISA, Enzyme-Linked Immuno-Sorbent Assay [2]. ELISA is a term referring to a similar group of tests rather than a single method of analysis [3]. The sandwich assay is a very common and representative method of ELISA testing [3].

There are four main steps to the sandwich assay. The procedures are carried out simultaneously on both unknown samples and a gradient of known samples to which a comparison will be made [3]. The assay has shown a very high degree of accuracy as all of the samples are treated the same throughout [2]. A 96-well plate is the principle substrate which consists of eight by twelve 2 mL polystyrene wells connected together in a rectangular matrix. The following outlines the procedure and lists some of the concerns associated with each step.

The first step is to secure the antibodies onto the polystyrene surface of the wells [3]. The chief means of immobilization is through adsorption [3]. Polyclonal antibodies are dissolved in PBS, a phosphate buffered saline with a non-denaturing pH of 7.2 - 7.4 [4]. The solutions are then pipetted into the wells where they sit for one hour [3]. The excess solution and unadsorbed antibody are then removed by washing in PBS and extracting the waste material [3].

As mentioned, the binding mechanism associated with the wells is adsorption. Figure 5 shows how the antibodies can stick to the surface of the substrate in various orientations. It should be noted that not all of the applied antibody is adsorbed to the well surface. Each well can adsorb a maximum of 100 ng when 1 µg of antibody solution is applied [3]. There is also the concern that adsorption renders some of the active sites of immobilized antibodies sterically hindered or inert [4]. Therefore, all of the wells, whether prepared for known or unknown samples, are treated with the same amount of antibody solution. Consequently, the gradient of known concentrations provides an estimate which factors in the polystyrene binding capacity and non-specific adsorption effects (binding in undesirable orientations).

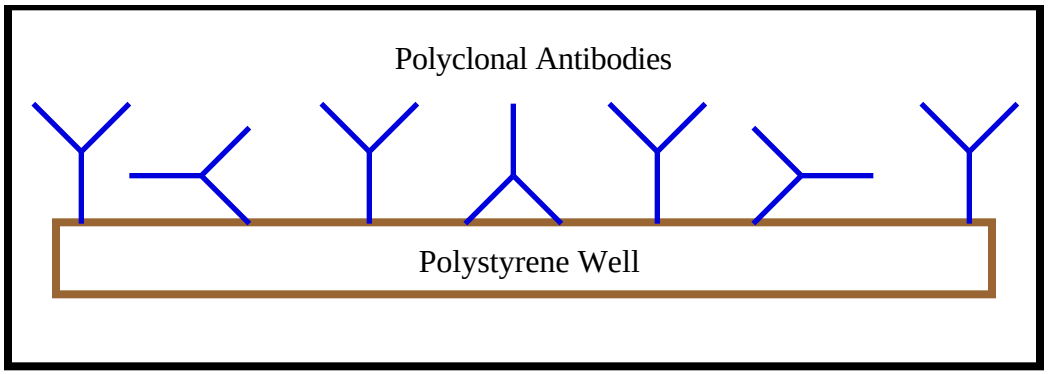

Figure 5: Polyclonal antibodies adsorbed onto a polystyrene substrate.

The second step, as shown in Figure 6, involves the addition of a blocking agent and the antigen samples, both dissolved in PBS [3]. The blocking agent is added to adsorb to any surfaces left untouched by the antibody [4]. Bovine serum albumin, or BSA, is commonly used [4]. It is during this second step where a gradient of known antigen concentrations is added to the comparison well groups [3]. The unknown samples are deposited to the rest of the treated wells [3]. The application of blocking agent and antigen samples can be combined due to the high affinity of the blocking agent for the substrate and the high affinity of the antigen for the antibody [4]. The solutions are allowed to incubate for one hour after which the excess is removed by washing in PBS [3]. Though it should be noted that the antigen will only bind with the active sites it can physically access, the following illustrations show only the interactions of interest.

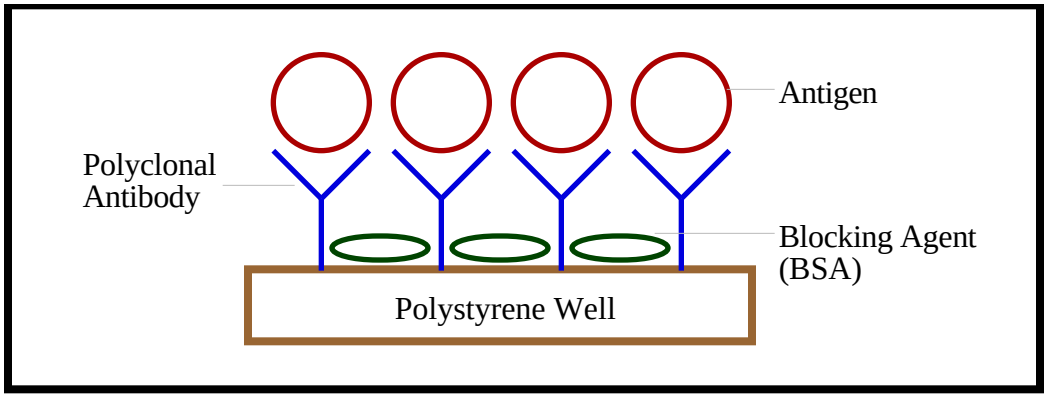

Figure 6: Addition of antigen samples and blocking agent in a sandwich immunoassay.

Figure 7 illustrates how in the third step, a second solution of antibodies is added to the system in a similar manner as the first [3]. The solutions are made up of monoclonal antibodies labeled with horseradish peroxidase, or HRP [3]. Labeling is paramount to most ELISA procedures. The term "Enzyme-Linked" refers to the chemical, fluorescent, or radioactive labeling necessary to the third step of the assays [3]. Labeling of antibodies is a delicate, time-consuming, sometimes expensive procedure [3]. The end result demands equipment such as spectrophotometers or scintillation counters which increase the overhead cost. In addition, because the first layer of antibodies was polyclonal, it is possible that some of the original antibodies are duplicated. Therefore, some of the monoclonal antibodies may not be able to bind to the antigen as their sites may be occupied. It is also possible that some of the antigen bonding sites are physically inaccessible.

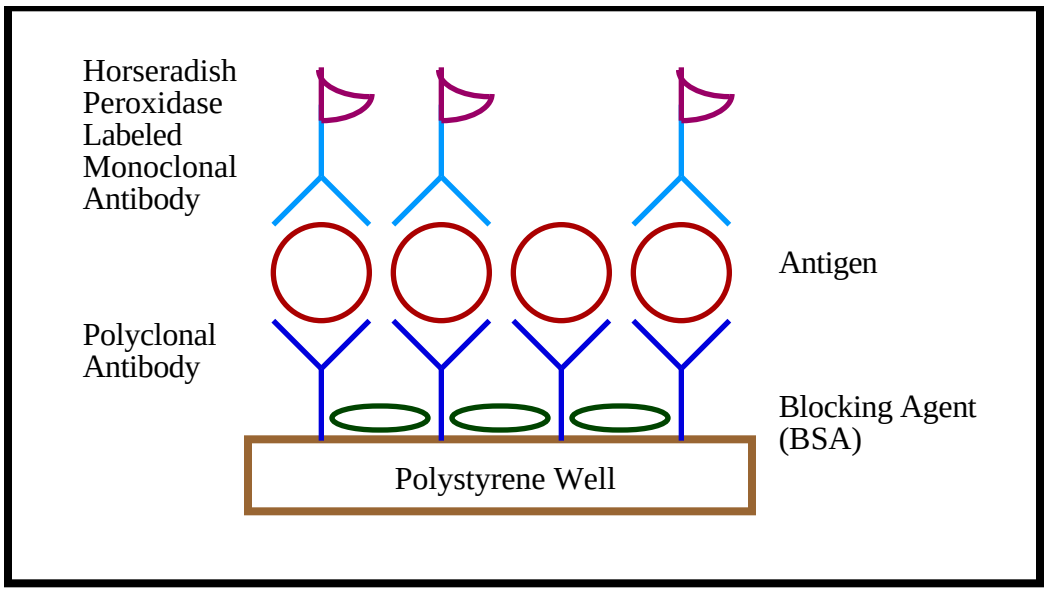

Figure 7: Addition of HRP labeled monoclonal antibody in a sandwich immunoassay.

In the fourth step, the system is probed as per the labeling scheme used on the monoclonal antibody [3]. For chemical labeling, such as in the sandwich assay, further chemical treatment is performed to initiate color changes which will be analyzed with a spectrophotometer. In Figure 8, the system is treated with hydrogen peroxide (H_2O_2), 3,3'5,5'-tetramethyl benzidine (TMB), and sulfuric acid (H_2SO_4) for a total of one hour [3]. The result yields color changes from clear to blue to yellow proportional to the amount of HRP bound to the system [3]. The spectrophotometer reading

to yellow proportional to the amount of HRP bound to the system [3]. The spectrophotometer reading absorbance at 450 nm gives a fairly accurate indication of the amount of antigen present in the samples [3]. The test samples are compared to the gradient of known antigen concentration [3]. From the comparison, it is possible to obtain a positive or negative test as well as a reasonable estimate of the antigen concentration in the test samples.

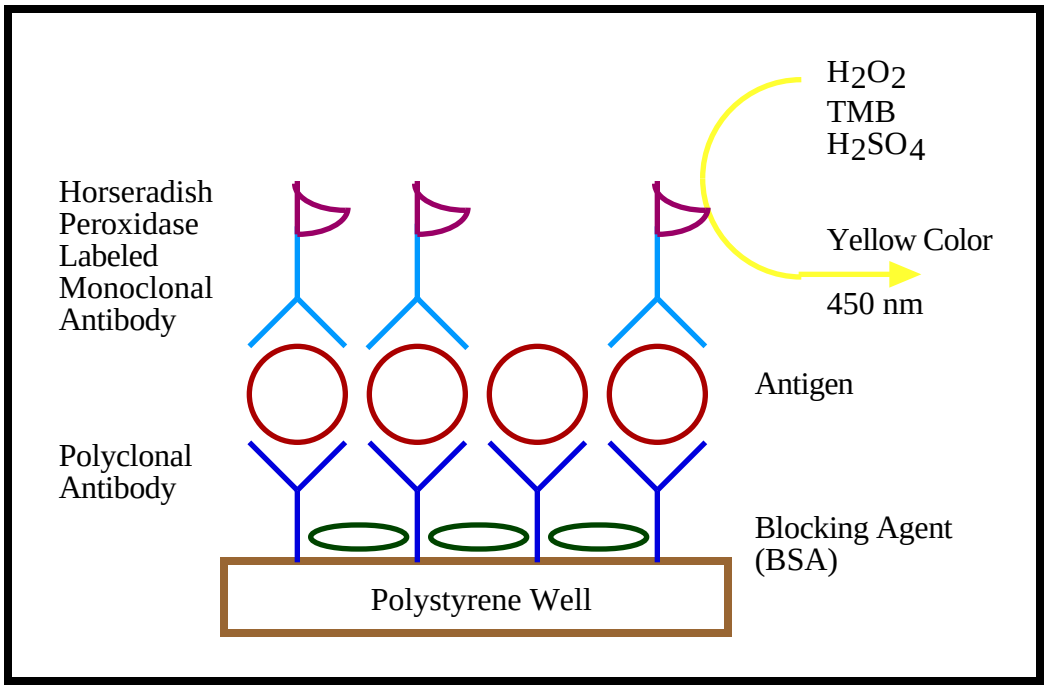

Figure 8: Addition of chemical indicators in a sandwich immunoassay.

2.2.3 OPTICAL SENSING TECHNIQUES

Though ELISA's are capable of high sensitivities, the time required to perform such an assay is significant. The expensive and delicate process associated with the labeling of antibodies is a concern. Polystyrene binding capacity and non-specific adsorption effects also offer drawbacks to the ELISA. Optical sensing techniques can be employed to eliminate some of these problems. The unreactive nature of the glass substrate of optical systems demands covalent binding techniques which offer better efficiency over adsorption. In addition, optical techniques can offer real-time results in a short period of time, sometimes eliminating the need for labeled secondary antibodies.

One proven optical technique for immunoassays is surface plasmon resonance, or SPR. Materials which behave similarly to the free electron model, such as metals, contain electrons which can be excited into a resonance condition [6]. In the resonance condition, incident radiation on the order of 633 nm couples the Fermi level electrons into a vibrational excited energy state creating a standing wave surface plasmon along the surface of the metal [6]. The surface plasmon is an evanescent wave which attenuates rapidly as it traverses the material [6]. The condition for excitation demands that the tangential wave vector component of the incident radiation equals the magnitude of the plasmon wave vector which exists along the metal interface [7]. In other words, the condition for resonance is not only dependent on the frequency of the incident radiation and the refractive indices of the metal and external medium, but also on the angle of incidence.

To operate the sensor, the metal is deposited onto the base of a glass prism [8]. Through additional binding chemistry, the antibody is immobilized onto the metal [8]. Blocking agent and sample can then be added in a single step [4]. Light is launched into the prism through a range of angles, as shown in Figure 9 [7]. The thickness of the metal layer is kept below 60nm, less than the penetration depth of the plasmon, allowing the wave to interact with the external medium. If the refractive index of the medium is changed (via antigen bonding to antibody), the angle of incidence required for resonance is also proportionately changed [7]. Since the creation of a plasmon initiates an evanescent wave, there will be a decrease in the intensity of the reflected light once resonance is reached [7]. By monitoring the angle at which the reflected light is attenuated, changes in the effective index of the medium can be determined.

Surface plasmon resonance offers several advantages over the ELISA. As the sensor detects changes in refractive index, the second layer of labeled antibody is unnecessary. Continuous monitoring of the device after the addition of the antigen sample offers the possibility of real-time analysis. The need for covalent binding offers two more advantages. In addition to better binding efficiency over adsorption, covalent binding gives rise to reusability. After an assay, a slightly acidic wash will disrupt the antigen-antibody bond but leave the antibodies permanently affixed to the metal surface without harming their active sites [2]. The disadvantages to SPR are few: the sensor is intensity based, and it is difficult to avoid moving parts in the detection system.

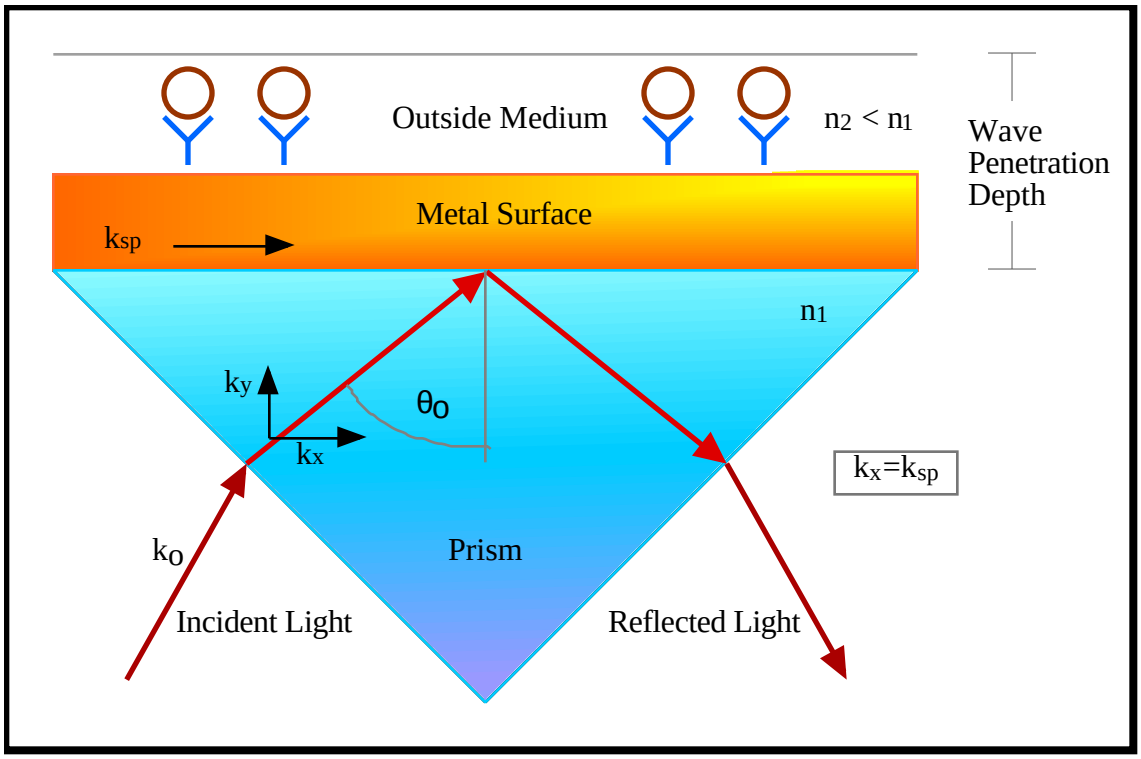

Figure 9: Model of surface plasmon resonance. [7]

Figure 10 demonstrates another optical technique which employs multi-mode optical fiber. The tapered fiber sensor, like the SPR device, makes use of evanescent fields and covalent binding. The cladding of the fiber is removed, and the exposed core is treated in hydrofluoric acid to etch it into a tapered shape [2]. The physically modified core is then chemically treated to allow immobilization of the desired antibody [2]. The test sample is a fluorophore-antigen complex which fluoresces when excited by light at 514 nm [2].

The assay is performed in a solution of phosphate buffered saline (PBS) in which the fiber is immersed [2]. Light from an argon-ion laser (514.5 nm) is launched into the core and carried to the tapered tip [2]. The aqueous solution acts as a cladding to the core allowing high order modes to interact with the antibody-antigen bond [2]. The light from the high order modes extends less than a wavelength from the core surface, allowing only the bound fluorophore-antigen complex to become excited [2]. The fluorescent light is coupled into the core and carried back to a detection system [2]. With a chopper, lock-in amplifier, and a system of lenses and filters, the return signal is analyzed to determine the amount of bound antigen [2].

is analyzed to determine the amount of bound antigen [2].

The tapered fiber sensor has some of the same advantages as the SPR device. Covalent bonding of the antibody and the ability to conduct real-time analysis name a few of the benefits. The use of a long fiber optic cable allows the biochemical interaction to take place away from the detection equipment, reducing the possibility of contamination of the equipment or the assay [2]. However, the fragility of the sensor, the need for fluorescent labeling, and the delicate nature of sensor fabrication prove to be liabilities. The shape of the tapered core must be designed for maximum fluorescent coupling, but V number mismatch at the cladding-solution interface causes some of the signal to be unavoidably lost [2]. In addition, great care must be taken to avoid erroneous results from ambient light interference [2].

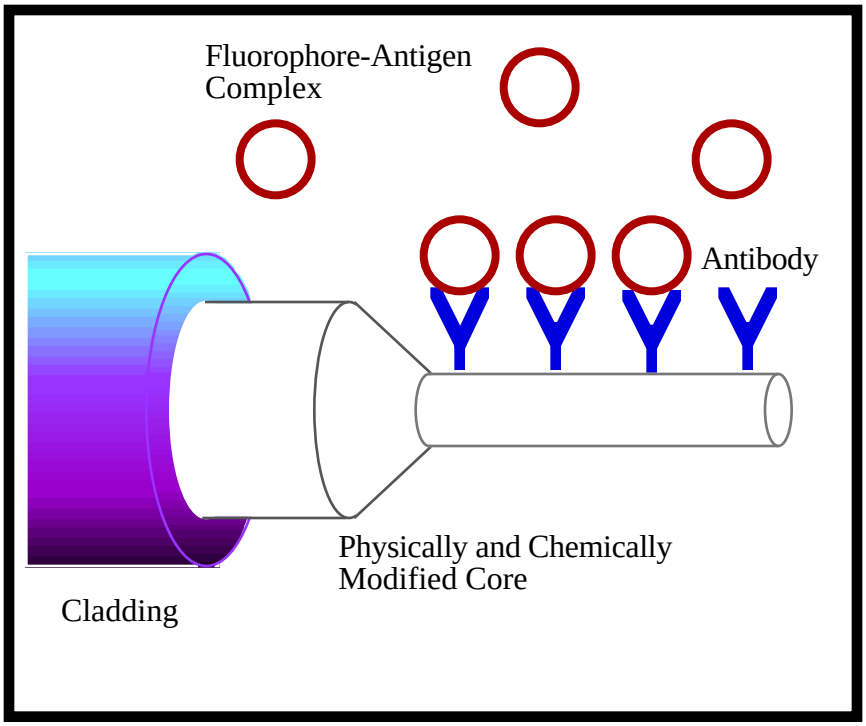

Figure 10: Tapered fiber optical sensor for immunoassays. [2]

In conclusion, the ideal immunoassay would offer the following capabilities:

- Elimination of second layer of antibodies,
- Elimination of labeling of biochemical reagents,
- Covalent binding of the antibody to the substrate,

- Reusability of the sensor,
- Ability to conduct real-time analysis,
- Easy sensor fabrication,
- A reliable, simple, inexpensive detection system,
- A sturdy, robust, inexpensive sensing instrument,
- Remote sensing ability to avoid contamination.

The long-period grating biosensor achieves most of these goals.

3.0 LONG-PERIOD GRATING BACKGROUND

This chapter outlines some of the basic properties of long-period gratings. Insight into the fiber Bragg grating is also offered as it applies to the understanding of these devices. Refractive index sensitivity to materials in contact with the cladding of the fiber is explained with wave propagation plots (β-plots) and wavelength versus grating period curves (λ vs Λ curves).

3.1 OVERVIEW

In general, a fiber grating couples light from one guided mode into another mode [10]. Fiber gratings are manufactured by writing a diffraction grating into the core of a photosensitive optical fiber [10]. Coupling between modes occurs when the phase matching condition is met [11]:

$$(k_c - k_m) + k_g := 0, \tag{3.1}$$

where k_c and k_m are the wave vectors of the affected modes and k_g is the momentum of the grating. In terms of the effective index, n_{eff}, seen by each mode and the period, Λ, of the grating, equation (3.1) can be rewritten as [11,12]:

$$\left(\frac{\omega \cdot n_{eff,\,c}}{c} - \frac{\omega \cdot n_{eff,\,m}}{c}\right) + \frac{2 \cdot \pi \cdot N}{\Lambda} := 0, \tag{3.2}$$

with ϖ as the frequency of operation, c the speed of light, and N the order of the grating. The difference in propagation constants of the coupling and coupled modes is denoted by Δß, thus simplifying the above equations for a first order grating to [11,12]:

$$\Delta ß := 2\pi / \Lambda. \tag{3.3}$$

Many types of fiber gratings have been demonstrated in the past, but only the fiber Bragg grating (FBG) and the long-period grating (LPG) will be detailed here [12]. FBG's operate by coupling light from the forward propagating fundamental mode of a single mode fiber to the reverse propagating fundamental mode [11]. The coupling is wavelength dependent and serves to create a mirror to a very specific frequency band. LPG's couple light from the forward propagating

mirror to a very specific frequency band. LPG's couple light from the forward propagating fundamental mode to several discrete forward propagating cladding modes [10]. Due to the spatial distribution of the fundamental mode, only the circularly symmetric cladding modes offer adequate modal overlap to facilitate coupling [10]. As there are imperfections in the cladding surface, these modes attenuate quickly leaving a series of loss bands in the output [12]. Figure 11 shows the difference in the transmission and reflection spectrums of both gratings.

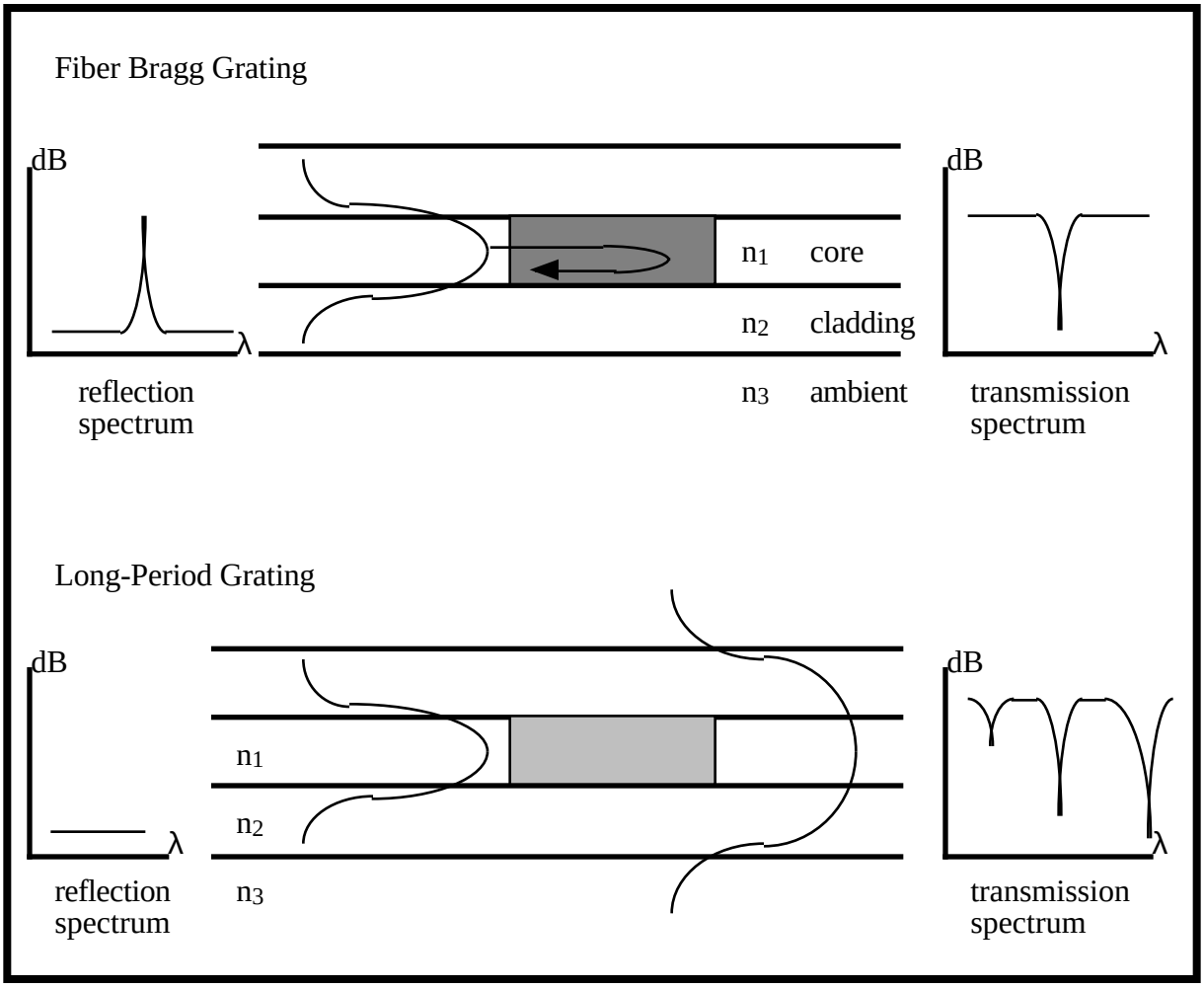

Figure 11: Transmission and reflection spectra of fiber Bragg gratings and long-period gratings.

3.2 ß-PLOTS

Gratings are sometimes described by the ß-plot representations shown in Figure 12 [12]. In a ß-plot, the propagation constants of the core and cladding modes are charted along a straight line. Modes given to the right of the origin are forward propagating, and modes given to the left are reverse propagating. The Δß arm connecting the coupling and coupled modes demonstrates the necessary phase matching condition. For Bragg gratings, the Δß arm is large requiring a short period (hundreds of nanometers) [13]. Conversely, for long-period gratings the period is forced to be large (hundreds of microns) to compensate for the small modal wave vector differential [13].

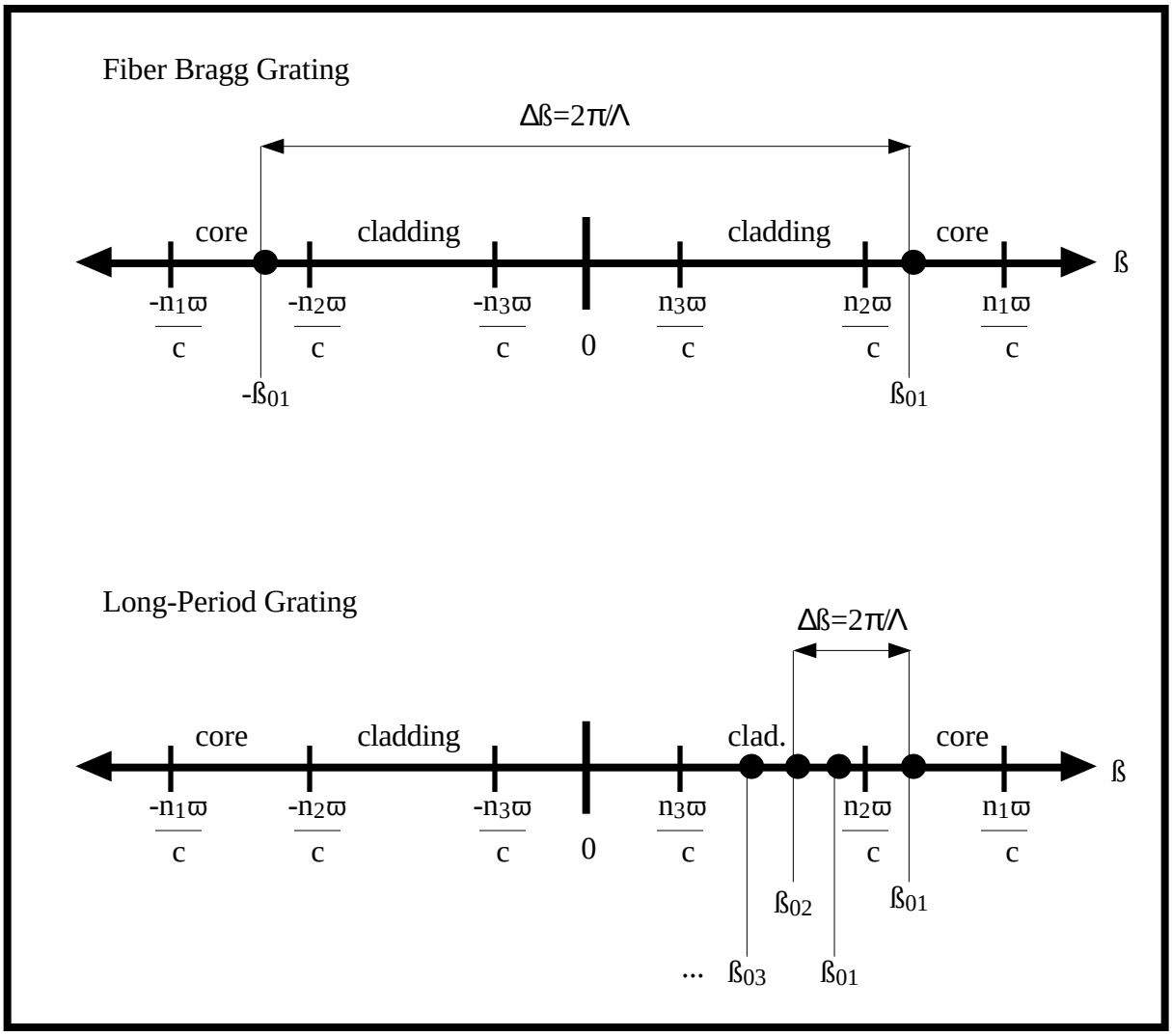

Figure 12: ß-plots for fiber Bragg gratings and long-period gratings. [13]

In figure 12, only one $\Delta ß$ arm is shown for the long-period grating though coupling occurs to several cladding modes. To demonstrate the multiple coupling effect, the ß-plot needs to be understood as a lay out of propagation constants for a specific wavelength. If the radian frequency is increased or decreased, the ß-plot is stretched or compressed as the wave vectors vary proportionally to ϖ [13]. The $\Delta ß$ arm dependent on the constant period remains fixed as the different cladding modes move into proper alignment for the phase matching condition. As an example, if one wished to show coupling to the $ß_{03}$ cladding mode instead, decreasing ϖ would compress the ß-plot until the third order cladding mode was separated from the fundamental core mode by $2\pi/\Lambda$. As a result, in the transmission spectrum, losses occurring at higher wavelengths, or lower frequencies, are attributed to higher order mode coupling for a fixed period.

The idea of resizing the ß-plot to meet the phase matching condition can be used to demonstrate the refractive index sensitivity of the LPG under normal operation [13]. As the fundamental mode is mostly confined to the core of the fiber, the medium outside the cladding has little influence on the effective index seen by the core mode [13]. Consequently, Bragg gratings show little response to refractive index changes of the surrounding medium unless the cladding is etched. Long-period gratings, on the other hand, couple light into evanescent cladding modes which do extend several nanometers beyond the fiber surface [12]. The effective index seen by the cladding modes involves the index of the surrounding material as well as the wavelength dependent index of the cladding [13]. If a material other than air comes into contact with the fiber at the location of the grating, an overall increase in the effective index is seen by the coupled cladding modes [13]. The added material increases the propagation constants, moving them to the right on the ß-plot. The frequency, in turn, must be increased, stretching the ß-plot until the phase matching condition is met. In practice, under normal operation, application of a material to the grating results in a shift of the loss bands to lower wavelengths. The spectral shift is monitored to determine the index of refraction of the surrounding medium.

Finally, the ß-plots can give insight as to how the loss bands of long-period gratings are formed during the normal fabrication process. The photo-induced index changes which take place in the core raise the effective index seen by the fundamental guided mode [13]. The propagation constant

of the core mode increases, moving its wave vector to the right on the ß-plot. A decrease in ϖ to meet the phase matching condition corresponds to loss bands which move to higher wavelengths as the grating is formed. A more detailed explanation of the fabrication process is given in section 4.1.

3.3 λ VS Λ CURVES

In this section, a second model is described which explains grating behavior more completely. Equations and computer modeling demonstrate the power of the λ vs Λ curves.

3.3.1 BASIC EQUATIONS

During fabrication of the long-period gratings, a region of anomalous operation was discovered when smaller periods were used (below 150 μm). In contrast to what can be intuited from the ß-plot, the loss bands moved to lower wavelengths as the grating was written and to higher wavelengths when material was applied to the cladding surface. Another model was investigated to explain long-period grating behavior in both modes of operation. The λ vs Λ curves were generated to characterize which periods produced which behavior [13].

To construct the λ vs Λ curves, a slightly different approach is taken to equation (3.3). Δß is expressed in terms of the propagation constants [12]:

$$\Delta ß := ß_{01} - ß^{(m)} = 2\pi / \Lambda, \tag{3.4}$$

where $ß_{01}$ is the propagation constant of the fundamental core mode, and $ß^{(m)}$ is that of the m^{th} order cladding mode. The following equations can be used to gain an accurate interpretation of the device behavior [13]:

$$ß_{01} := \sqrt{\left(\frac{2\cdot\pi\cdot n_1}{\lambda}\right)^2 - \left(\frac{u}{a}\right)^2}, \tag{3.5}$$

$$\beta_{01} := \sqrt{\left(\frac{2\cdot\pi\cdot n_1}{\lambda}\right)^2 - \left(\frac{u}{a}\right)^2}, \tag{3.5}$$

with the core radius, a, and u approximated as [13]:

$$u := \frac{\left(1+\sqrt{2}\right)\cdot V}{1+\left(4+V^4\right)^{\frac{1}{4}}}. \tag{3.6}$$

The normalized frequency, V, is defined by [13]:

$$V := \frac{2\cdot\pi\cdot a}{\lambda}\cdot\sqrt{\left(n_1\right)^2 - \left(n_2\right)^2}. \tag{3.7}$$

The m^{th} order cladding mode is found from [13]:

$$\beta^{<m>} := \sqrt{\left(\frac{2\cdot\pi\cdot n_2}{\lambda}\right)^2 - \left(\frac{j_m}{b}\right)^2} \tag{3.8}$$

where b is the cladding radius, and j_m is the m^{th} root of the zero order Bessel function ($J_o(j_m)=0$).

Using the above equations with fine tuning to address the wavelength dependent nature of the effective refractive indices and a more detailed treatment of changes which occur in the core during fabrication, a model was generated to predict the behavior of the long-period gratings [13]. Figure 13 shows the λ vs Λ curves obtained from the model for Corning Flexcor fiber with a cut-off wavelength of 1060 nm. The core and cladding diameters are 4 μm and 125 μm, and the core is doped with an average of 13.5% germanium [13]. Estimates of photo-induced changes within the core during fabrication were based on laser power, exposure times, and the degree of hydrogen loading [13]. Fabrication procedures are outlined in section 4.1.

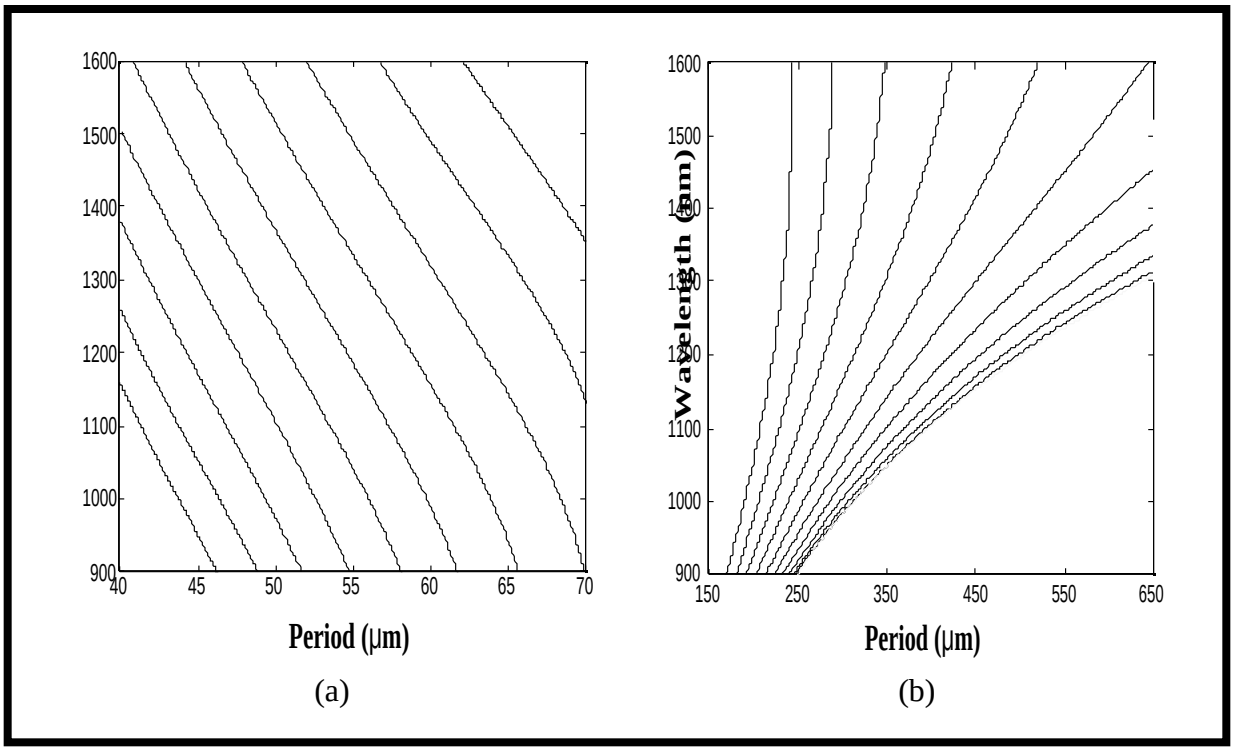

Figure 13: λ vs Λ curves for Corning Flexcor fiber (cut-off 1060 nm) in (a) anomalous and (b) normal operation. [13]

To use the graph, a horizontal line at the desired wavelength of operation gives the periods needed to achieve them, and a vertical line shows which modes and wavelengths will appear given a fixed period [13]. Each curve corresponds to a cladding mode as the period is varied and the phase matching condition is met [13]. The graphs of Figure 13 show highest order to lowest order modes from left to right [13]. High order modes written with smaller periods have negative slopes or points of inflection and are considered to be in the anomalous region of grating operation [13].

3.3.2 A QUALITATIVE ANALYSIS

To demonstrate the behavior of the device in both regions, a Mat lab program was written based on equations (3.4) - (3.8). Using realistic estimates of the parameters more carefully handled in the advanced model, a qualitative assessment of grating behavior can be determined. Figure 14 shows

the λ vs Λ curves generated with the program. Three modes are labeled: A is a first order cladding mode, and B and C are successively higher order modes.

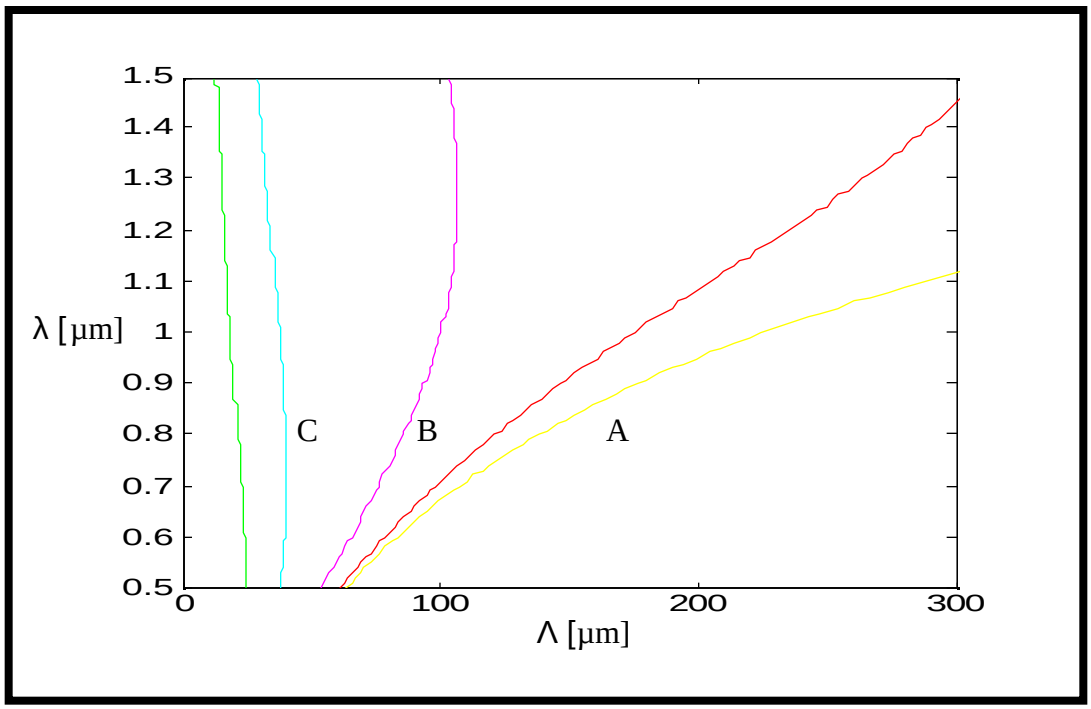

Figure 14: Qualitative λ vs Λ curves for long-period gratings.

Figure 15 demonstrates a simulation of what happens to each of the labeled modes when the effective index of the cladding is increased by the addition of an external medium. The same equations are used as in Figure 14, but only one mode per graph is shown as the cladding index is changed. An arrow indicates which direction the curves move when more dense materials are applied. The dashed lines reveal what occurs to each mode for a fixed period targeting an initial wavelength of approximately 1150 nm.

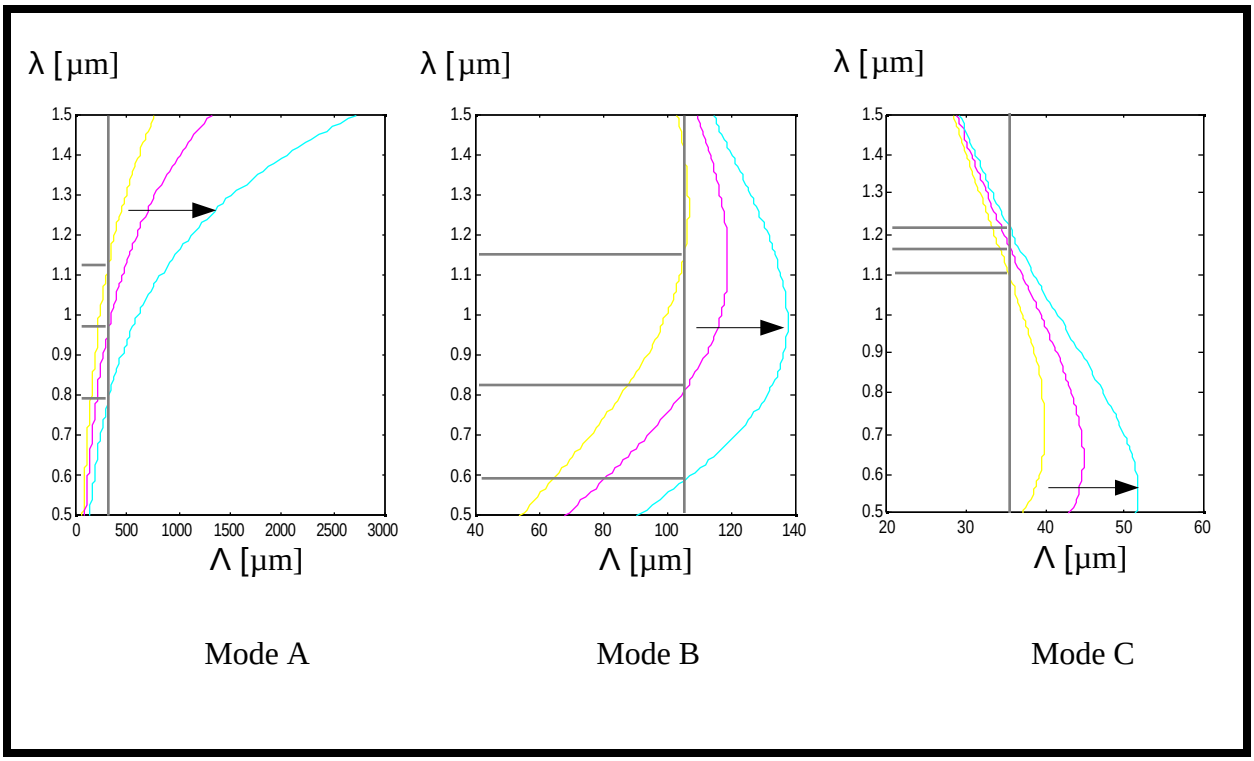

Figure 15: Qualitative results of increasing effective cladding mode index for modes pictured in figure 14.

For mode A in the region of normal operation, and for mode B at the inflection point, denser materials correspond to a negative spectral shift. Mode C in the anomalous region gives rise to larger wavelengths. The incremental changes of 0.002 per step are the same for each graph. A more detailed analysis would investigate how the higher order modes with additional power in the side lobes are slightly more affected by the index of the medium [13]. It is expected that the low order modes would show the least response to ambient index changes. However, the qualitative analysis agrees with experimental result; modes corresponding to curves of inflection on the λ vs Λ curve give rise to greater index sensitivity. Such modes could give rise to positive or negative spectral shifts depending on the wavelength of interest. A modal split is seen with some periods which cross the same mode at two different wavelengths.

3.4 FINAL NOTES ON REFRACTIVE INDEX SENSING

A final consideration of the index of refraction sensitivity of the long-period grating involves the range of indices to which the grating responds. Spectral shifts become more dramatic as the index of the surrounding medium approaches the effective index seen by the cladding mode in question [13]. To model the effect of the changing medium, equations (3.4 - 3.8) can be modified. If the core mode which is almost unaffected by the external medium is ignored, the model can be treated as a new fiber with the cladding as the core and the outside material as an infinite cladding [13]. Substitution of n_2 and n_3 for n_1 and n_2, ∞ for b, and b for a, yields the following equations:

$$\Delta\beta = \beta_{core} - \beta_{clad} = 2\pi / \Lambda, \tag{3.9}$$

$$\beta_{core} := \sqrt{\left(\frac{2\cdot\pi\cdot n_2}{\lambda}\right)^2 - \left(\frac{u}{b}\right)^2}, \tag{3.10}$$

$$u := \frac{\left(1 + \sqrt{2}\right)\cdot V}{1 + \left(4 + V^4\right)^{\frac{1}{4}}}, \tag{3.11}$$

$$V := \frac{2\cdot\pi\cdot b}{\lambda}\cdot\sqrt{\left(n_2\right)^2 - \left(n_3\right)^2}, \tag{3.12}$$

$$\beta_{clad} := \sqrt{\left(\frac{2\cdot\pi\cdot n_3}{\lambda}\right)^2}. \tag{3.13}$$

The quadratic nature of the above equations gives rise to greater wavelength shifts as the index of the ambient material approaches the effective index of the cladding. When n_3 equals n_2, the V number reduces to zero. In turn, u is reduced to zero, and the $\Delta\beta$ term disappears. The result is a resonance condition in which the loss band is nonexistent [13]. The ambient material and the cladding form a continuous waveguide structure [13]. Core modes are coupled to a continuum of radiation modes giving an overall 2 - 3 dB loss across the entire transmission spectrum [13]. When

When n_3 exceeds n_2, V and u become purely imaginary. The $\Delta\beta$ term remains real but virtually unaffected by increases in n_3 [13]. The result is a return of the loss band but with imperceivable spectral shifts as the index of the medium escalates beyond the effective index of the cladding [13].

Figures 16 - 18 show experimental results of index of refraction testing representative of the modes offered in Figure 14 for Corning Flexcor fiber. A period of 40 μm yields gratings operating on the negative slopes of the λ vs Λ curves, a 120 μm period operates on an inflection point, and a 200 μm period involves the positive, more gradually sloped, lower order modes. Gaps in the plots correspond to the disappearance of the loss bands at resonance. Resonance is reached at smaller refractive indices for the higher order modes owing to the difference in the effective cladding index seen by all of the modes [13].

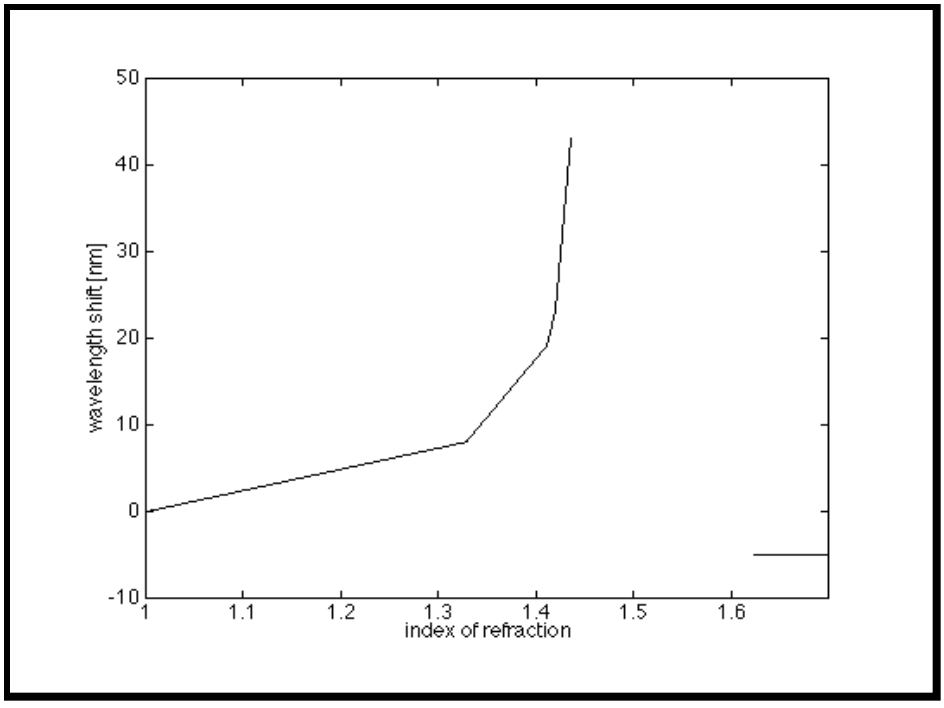

Figure 16: Results of refractive index testing on a 40 μm long-period grating written in Corning Flexcor fiber.

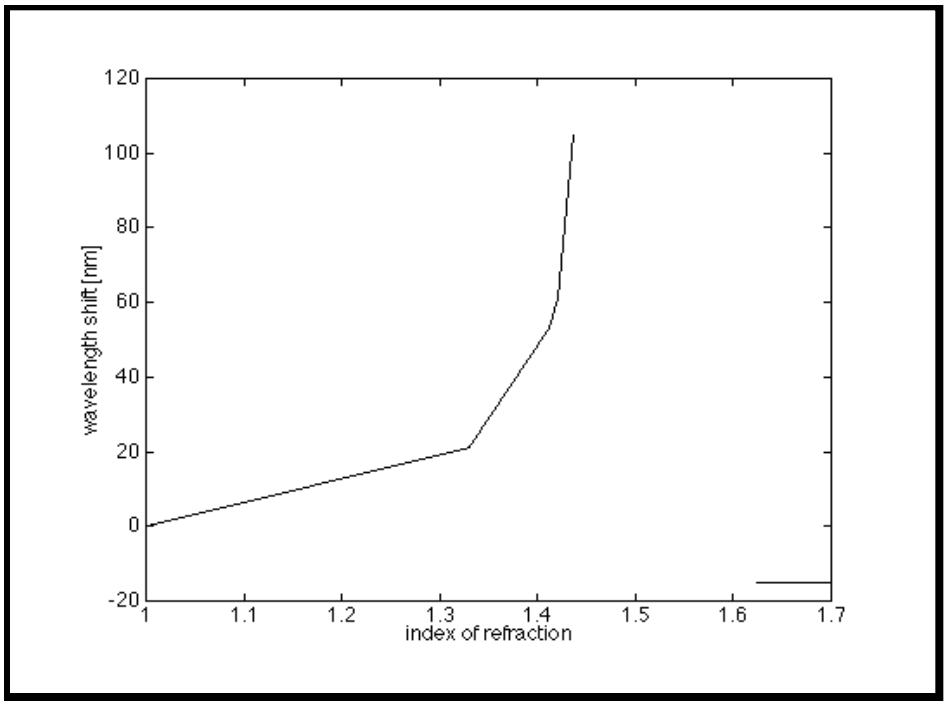

Figure 17: Results of refractive index testing on a 120 µm long-period grating written in Corning Flexcor fiber.

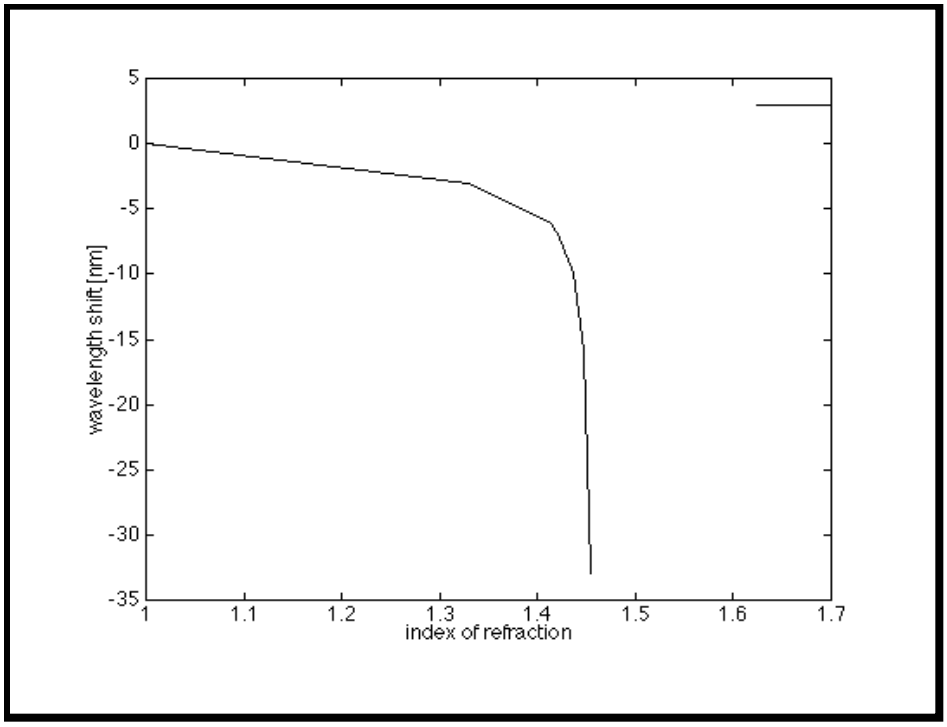

Figure 18: Results of refractive index testing on a 200 µm long-period grating written in Corning Flexcor fiber.

3.5 CROSS-SENSITIVITY

Fiber gratings are sensitive to temperature and strain variations as well as index of refraction changes [14]. Wavelength shifts during any testing procedure need to be verified and checked against cross-sensitivity to other phenomena. Gratings can be modified to reduce their response to temperature and strain, or these perturbations can be carefully controlled to obtain more accurate data [14,15].

Modification of equation (3.4) using the chain rule of derivatives gives the change in wavelength, λ, with the change in temperature, T [14]:

$$\frac{d\lambda}{dT} := \frac{d\lambda}{d\left(\delta n_{eff}\right)} \cdot \left(\frac{dn_{core}}{dT} - \frac{dn_{clad}}{dT} \right) + \Lambda \cdot \frac{d\lambda}{d\Lambda} \cdot \frac{1}{L} \cdot \frac{dL}{dT} \tag{3.14}$$

where δn_{eff} is the differential effective index between the core and cladding modes, and L is the length of the grating. The first term on the right is due to the material effects of temperature variations [14]. For optical fiber, the material effects are positive [14]. The second expression gives the waveguide contribution [14]. The waveguide effect can be forced negative by using smaller periods to write the grating [15]. As demonstrated in section 3.3, periods below 100 μm give rise to cladding modes which have a negative $d\lambda/d\Lambda$ slope on the λ vs. Λ plot. The order of the cladding mode and the wavelength of operation factor heavily into both terms [14]. By choosing an appropriate period, the temperature sensitivity of a grating can be greatly reduced as the material and waveguide effects cancel each other [15].

Long-period gratings have demonstrated 5 - 15 nm shifts with a 100°C change in temperature [15]. Gratings written with a 40 μm period in Corning Flexcor fiber give a 0.18 nm shift for the same temperature variation [14].

Application of axial strain, ε, causes wavelength shifts according to [14]:

$$\frac{d\lambda}{d\varepsilon} := \frac{d\lambda}{d\left(\delta n_{eff}\right)} \cdot \left(\frac{dn_{core}}{d\varepsilon} - \frac{dn_{clad}}{d\varepsilon} \right) + \Lambda \cdot \frac{d\lambda}{d\Lambda} \tag{3.15}$$

The response to strain is dependent on the material and waveguide effects [14]. Once again, the

The response to strain is dependent on the material and waveguide effects [14]. Once again, the order of the cladding mode and the wavelength of operation are important to both terms [14]. Lower order cladding modes give rise to a negative material contribution [14]. The waveguide contribution becomes positive due to the associated positive $d\lambda/d\Lambda$ slope. A sufficiently large period will cause the material and waveguide effects to cancel [14].

Typical axial strain responses in LPG's have demonstrated 20 - 25 nm wavelength shifts for 1%ε [14]. A 340 μm grating written in Corning SMF-28 fiber gives only a 0.4 nm shift for the same amount of applied strain [14].

4.0 IMPLEMENTATION

This chapter endeavors to explain the marriage of the technologies of long-period gratings and biochemistry into a viable sensor. Fabrication of the long-period gratings and the binding chemistry of antibody attachment are considered.

4.1 FABRICATION OF LONG-PERIOD GRATINGS

The first step in constructing the biosensor is to make the long-period grating. Corning Flexcor fiber with a cut-off wavelength of 1060 nm was selected for its low cost and high germanium content. The fiber has a step index profile easily analyzed by the developed grating model [13]. Its core and cladding diameters are 4 μm and 125 μm, and there is a 13.5% germanium doping in the core [13].

The fibers are placed in a hydrogen-filled chamber under a pressure of 1750 psi for four to seven days at room temperature [13]. The hydrogen loading serves to increase the photosensitivity of the core [11]. The mechanism by which the fiber is rendered more sensitive to ultra-violet light is not yet known in detail [11]. It has been proposed that it involves the existence of both GeO and GeO_2 in the core [11].

Without hydrogen loading, UV radiation frees an electron in the oxygen deficient sight, causing a local defect which raises the core index at that point [11]. Cerium, europium, erbium:germanium, and boron:germanium dopants also show similar properties, though germanium doping demonstrates the most photosensitivity [11]. A germanium doped core can exhibit index changes on the order of 10^{-3} with exposure to an excimer laser [11].

When hydrogen is forced into the core, it is believed that GeOH is formed upon irradiation [11]. The photo-chemical reaction causes permanent defects and an increase in the core index at the exposed sites [11,13]. All of the GeO at these sites undergo the transformation yielding core index

changes greater than 10^{-2} [11].

Once loaded, the fibers are exposed to periodic UV radiation with the fabrication facility shown in Figure 19. Ultra-violet light from a frequency doubling argon ion laser is reflected at 45˚ and passed through a cylindrical lens which focuses the beam onto the axis of the fiber. An amplitude mask with a 50% duty cycle is placed in the path of the beam. Phase masks are used similarly for the manufacture of Bragg gratings. A jacket-stripped section of fiber is held tightly against the mask at the focal point of the lens. The mirror and lens are then translated along the length of the grating. As the beam dimensions are small, the translation of the mirror-lens assembly allows a longer grating to be written and also permits consistent, even index changes along its length. The formation of the loss bands is monitored using a light source and optical spectrum analyzer.

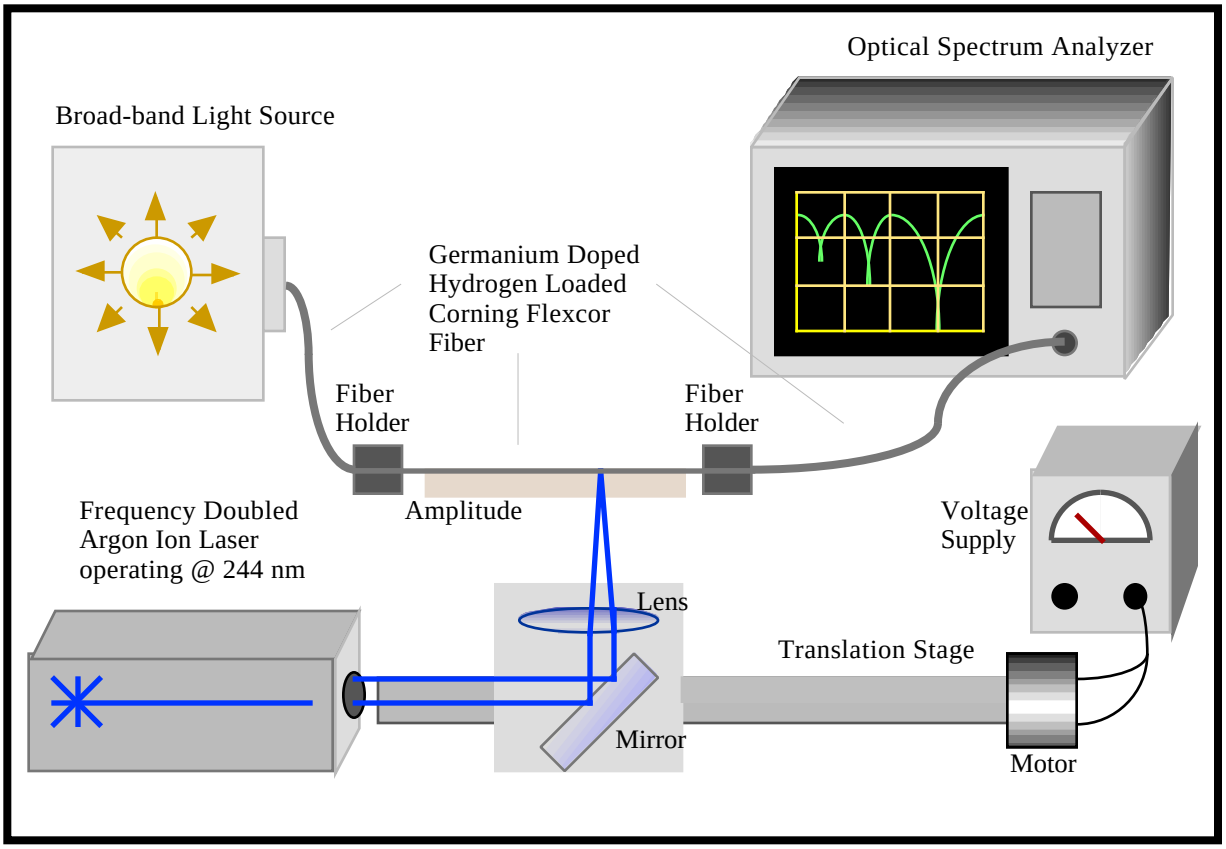

Figure 19: Long-period fabrication set-up.

Several factors need to be considered during fabrication. The choice in period, the length of the

Several factors need to be considered during fabrication. The choice in period, the length of the grating, laser intensity, grating length vs. laser intensity profile, and exposure time affect the placement and shape of the loss band [13]. All of the above parameters contribute to the magnitude of the photo-induced index variations within the core [13]. As the effective index seen by the fundamental propagating core mode changes, the phase matching condition is affected as well as the wavelengths required for mode coupling.

The rectangular shape of the resulting core index profile shown in Figure 20 gives rise to a sinc-squared function in the spectrum, as a Fourier transform of the spatial function into the frequency domain would predict. Similarly, the longer the grating, the thinner the loss band. Typical lengths range from one to two centimeters. Longer gratings would give a more desirably thin isolation, but exceeding two centimeters presents a problem particular to sensors. It is necessary to have the outside perturbation consistent along the length of the grating to get accurate sensor feedback, which becomes more difficult as the area to be covered increases. As long as the laser output power remains constant, chirping which would widen the band can be avoided [13]. Two centimeter gratings can achieve a sufficient full-max-half-power of 20 nm.

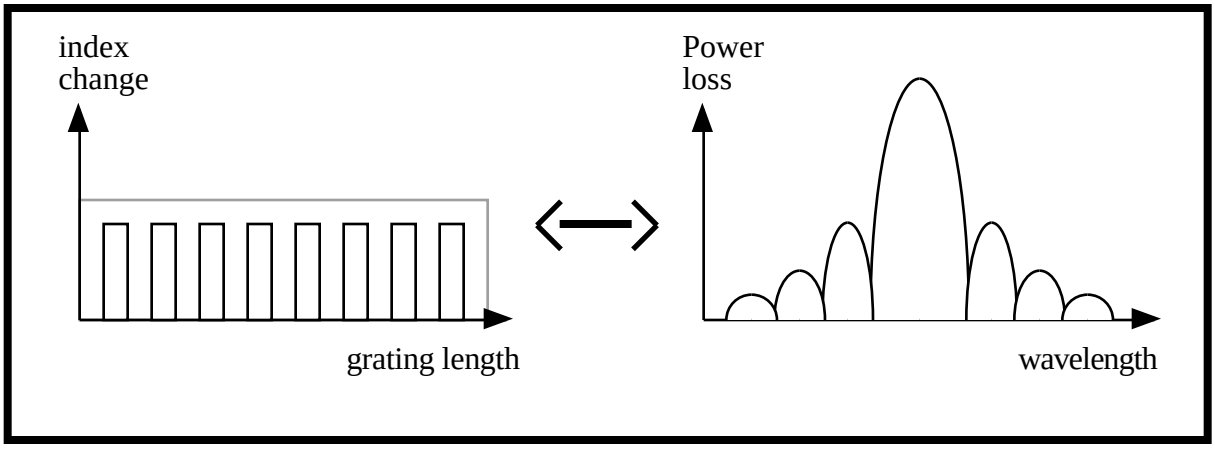

Figure 20: Relation of index change profile to shape of loss band in transmission spectrum.

Overcoupling corresponds to power being coupled back into the core causing the loss band to shrink [13]. It is primarily dependent on laser intensity, exposure time, and the length of the grating [13]. Higher order modes overcouple first, followed in turn by the lower order modes. As the

the grating is written, the desired mode is allowed to grow to the verge of overcoupling so that maximum power transfer is achieved. Modal overlap with the core and thus the order of the mode determines the maximum value of the loss band [13]. Better overlap in the sixth to tenth order modes gives rise to 40 - 60 dB losses [13]. Other modes may yield as little as 10 dB. As mentioned in section 3.2, as irradiation locally increases the core refractive index, the overall effective index seen by the fundamental mode is increased. Figure 21 demonstrates how the modes move to higher wavelengths as they are formed under the normal region of grating operation [10]. The opposite effect is seen under the anomalous region.

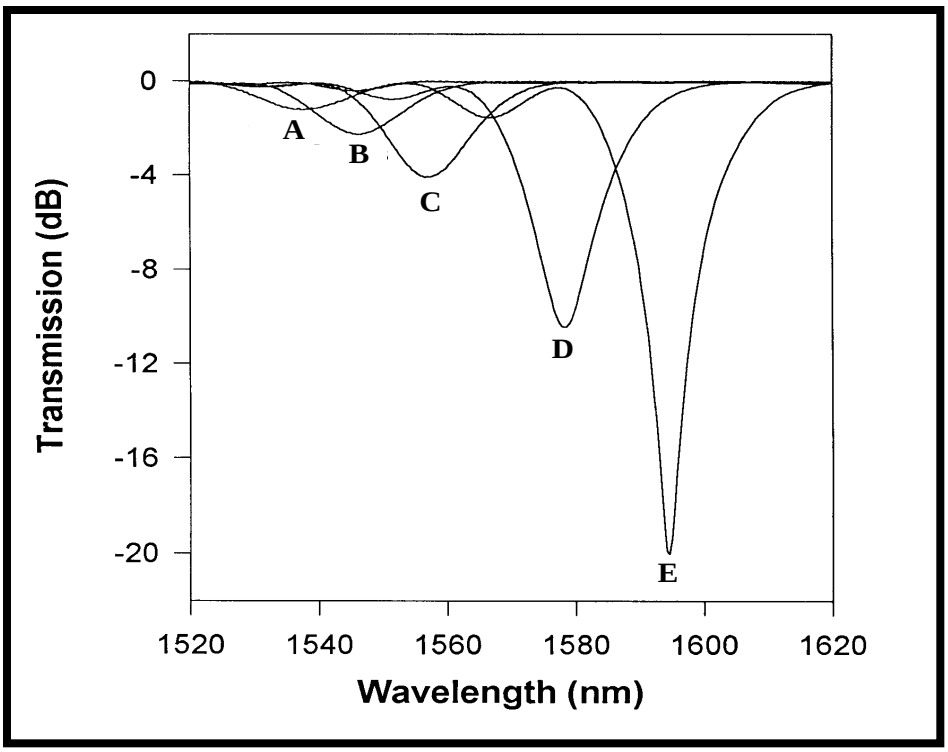

Figure 21: Loss band forming during long-period grating fabrication.
Each step corresponds to one minute of ultra-violet exposure time. [10]

The final step to LPG fabrication is to anneal the grating at 200˚C for five to eight hours [13]. Annealing forces the unreacted hydrogen to diffuse out of the fiber [13]. The loss of hydrogen decreases the effective core index, causing the loss bands to shift to lower wavelengths (normal operation) [13]. Annealing also stabilizes the UV induced defects left by the fabrication process [13]. Though the effects of hydrogen diffusion would cease after 24 hours, the UV induced defects

defects would impact the spectral placement of the loss bands for hundreds of hours [13]. Annealing serves to give the grating thermal stability in an accelerated amount of time. Figure 22 shows the difference annealing makes. Note that for the grating left at room temperature, the data is able to show the loss band shifting first to larger wavelengths and then to lower ones. The initial diffusion of hydrogen is from the cladding into the core to reach equilibrium within the glass [13]. The final shifting trend in part reflects the hydrogen leak into the atmosphere to reach a steady-state there [13].

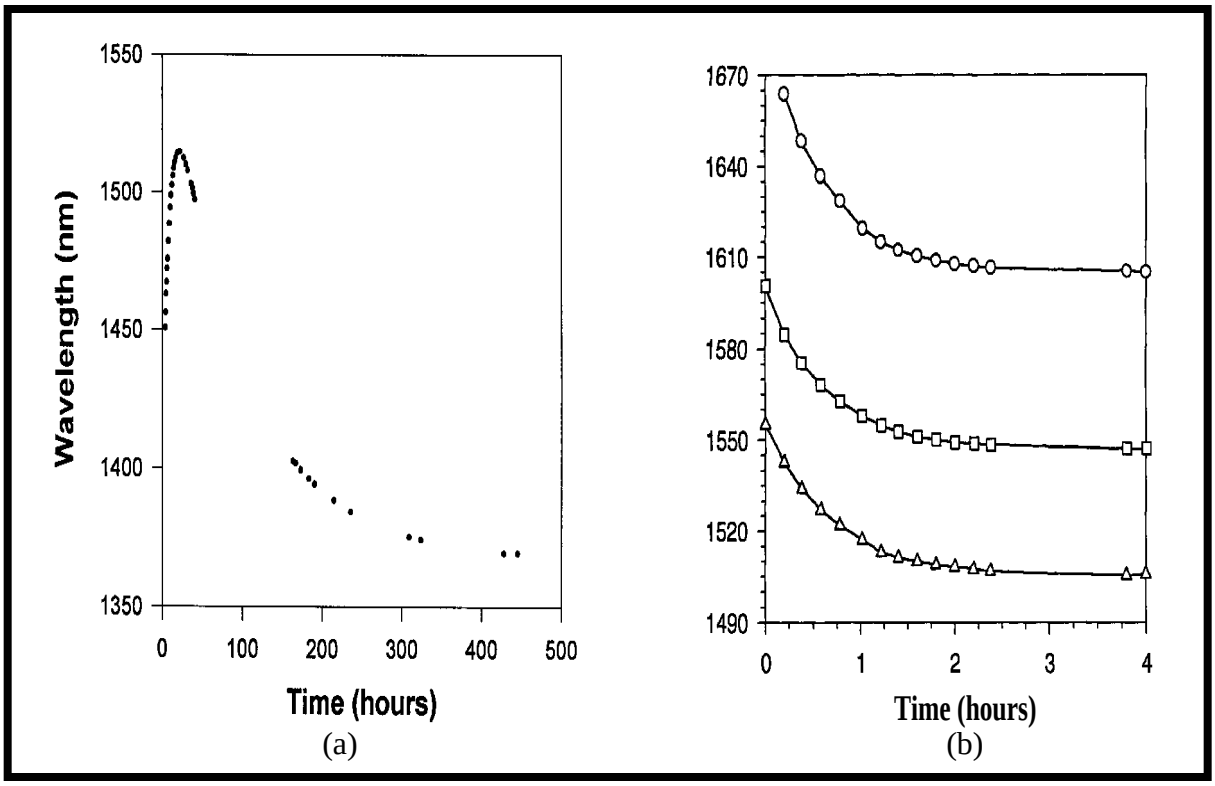

Figure 22: Spectral shift of LPG (a) left at room temperature vs (b) during annealing at 200°C. [13]

4.2 CHEMICAL BINDING OF ANTIBODY TO SILICA

4.2 CHEMICAL BINDING OF ANTIBODY TO SILICA

This section outlines various procedures to bond antibodies to the glass surface of the grating. A silane-crosslinker approach is detailed which connects the cladding to the Fc portion of the antibodies through a series of covalent bonds.

4.2.1 EARLY ATTEMPTS

At the beginning of this research, attempts were made to adsorb the antibodies directly to the cladding surface. As the cladding is made of rather unreactive glass, the attempts failed. A search was conducted to determine a way in which the antibodies could be permanently secured to the sensor.

Adsorption through a copolymer was researched but rejected. With adsorption, there is the possibility that some of the antibody could be denatured or washed off during the assay [4]. As there is little surface area to bond to, $2\pi rL = 125\ \mu m \times \pi \times 2\ cm = 7.85\ mm^2$, loss of antibody is highly undesirable. It was decided that some amount of covalent bonding was necessary.

When experiments with the silane-crosslinker procedure (detailed in section 4.2.2) proved temporarily unsuccessful, another approach was considered which should be mentioned here. Adsorption coupled with covalent binding was researched and tested at the Fralin Technology Center at Virginia Polytechnic Institute & State University with the cooperation of the university's Fiber & Electro-Optics Research Center. The medium of this antibody interaction was a dextran hydrogel.

The dextran hydrogel procedure was developed to capture antibodies onto the flat surface of a prism for surface plasmon resonance experiments [9]. The necessary gold layer is deposited first to which a monolayer of 16-mercapto-1-hexadecanol is added [9]. The monolayer allows a dextran hydrogel to covalently bind to the system. The hydrogel forms a hydrophilic three

dimensional matrix [8]. Carboxymethyl groups within the matrix are activated to induce a negative charge which attracts the antibodies [9]. Researched results promised 50 ng/mm^2 of adsorbed antibody onto the flat surface [9].

Several attempts were made to perform the dextran hydrogel procedure on long-period gratings. The gold layer was left out as the method of detection did not involve surface plasmons. Absence of the gold layer allowed the antibody reaction to occur closer to the cladding surface of the grating. The procedure takes a total of four days of treatment and incubation before antibody and antigen can be introduced [3]. The results were inconclusive [3].

Antibody-antigen detection varied from analyzing the output of the sensor to performing ELISA tests on the fibers themselves. The gratings showed no significant response to the addition of antigen, and the chemicals involved with the procedure had the potential to interfere with the ELISA tests [3]. Further, the results of the ELISA assays were difficult to interpret as solid fibers were being compared to a gradient of aqueous solutions.

There are several theories on the failure of the dextran hydrogel method. Researched results show the dextran layer to be 100 - 200 nm thick, possibly too thick for the evanescent wave to interact with the antibody-antigen reaction [9]. The research also estimated the refractive index of the monolayer at 1.59 [9]. This could push the reaction outside of the sensing range if the monolayer is thick enough. It is also reasonable that the dextran layer did not bind successfully to the fiber. After several trials, the experiment was dropped.

4.2.2 SILANE-CROSSLINKER APPROACH

A silane-crosslinker technique was investigated which promised strict covalent bonding [4]. The antibody binds to a crosslinker attached to a silane layer which in turn is bound to the glass surface [4]. The procedure offered several possible combinations of silane and crosslinker.

The silane films investigated in the patent included 4-Aminobutyldimethylmethoxysilane (ADS), 1-aminobutyltriethoxysilane (ATS), mercaptomethylethoxysilane (MDS), 3-mercaptopropyl-trimethoxysilane (MTS), and 3-glycidoxypropyltrimethoxysilane (GTS) [4]. Each of the silanes bonded to a specific class of crosslinkers through various functional groups [4]. Based on contact angles with water droplets, MDS was the developer's silane of choice [4]. MDS bonds to a crosslinker through a terminal sulfhydryl group [4]. Based on the unavailability of this compound, MTS was chosen for this research effort due to its similar binding characteristics and contact angle performance [4].

Several crosslinkers were considered as well [4]. All of the tested crosslinkers are heterobifunctional; the molecules have two reactive sites which bond to two different functional groups [4]. Homobifunctional crosslinkers with two identical reactive sites could bind to the silane at both locales (given a long enough molecule) with no functional group left to capture the antibody. The goal of the crosslinking layer is to covalently bind to the primary amine group of the Fc portion of the antibody as well as to the reactive group of the silane [4].

The crosslinkers tested in the patent were N-γ-maleimidobutyryloxy succinimide ester (GMBS), N-succinimidyl-3-(2-pyridyldithio) propionate (SPDP), N-succinimidyl-(4-iodoacetyl)amino-benzoate (SIAB), and succinimidyl 4-(*p*-maleimidophenyl) butyrate (SMPB) [4]. Using MDS coated optical fiber and glass slides, the above crosslinkers were tested with rabbit anti-goat as the antibody layer [4]. The fibers and slides were then treated with BSA and goat IgG as the antigen [4]. The results for antigen attachment to the various crosslinkers is given in Table 1. GMBS was chosen for this research for its high specific antigen binding and low standard deviation.

Heterobi-functional crosslinker	Nonspecific antigen adsorption	Total antigen binding	Percentage specific antigen binding
GMBS	11 ± 3 ng	328 ± 17 ng 0.34 ng/mm^2	97%
SPDP	11 ± 2 ng	345 ± 70 ng 0.36 ng/mm^2	97%
SIAB	17 ± 4 ng	373 ± 63 ng 0.39 ng/mm^2	95%
SMPB	18 ± 2 ng	369 ± 109 ng 0.38 ng/mm^2	95%

Table 1: Reaction of various crosslinkers with rabbit anti-goat and goat IgG. [4]

The silane crosslinker procedure takes approximately three hours to perform [2]. In the first step, the fibers are treated in a 1:1 mixture of hydrochloric acid and methanol, followed by concentrated sulfuric acid, and then boiling distilled water [2]. The first step cleans the fibers and hydroxylates the surface [4]. Hydroxylation increases the hydroxyl groups available for silane attachment, making a hydrophilic environment [3].

In the second step, MDS is diluted in anhydrous toluene and applied to the fibers in an inert atmosphere [4]. The reaction is carried out in a glove box with a continuous flow of purified nitrogen. The inert atmosphere and anhydrous nature of the solvent allow the silane to react with the hydroxyl groups of the cladding rather than those of competing ambient moisture [4]. During the reaction, a proton and a methoxy group are displaced to form the covalent bond [4].

The third step involves the addition of the crosslinker [2]. GMBS is dissolved in a minimal amount of dimethylformamide (DMF) which in turn is diluted with absolute ethanol [4]. The DMF is a non-aqueous, non-polar solvent which brings the crosslinker into solution [16]. The purity of the ethanol ensures that the competing hydrolysis reaction of the dissolved crosslinker does not override the reaction with the silane [16]. The thiol-terminal MTS reacts with the GMBS through

the crosslinker's maleimide functional group [4]. The succinimide functional group is left free to react with the primary amine of the Fc portion of the antibody [4].

All of the reactions take place through covalent binding [4]. The structure of the components of the linking layers is given in Figure 23. The result of the silane-crosslinker procedure is summarized in Figure 24. The thickness of each layer is estimated to be below 150 Å [5].

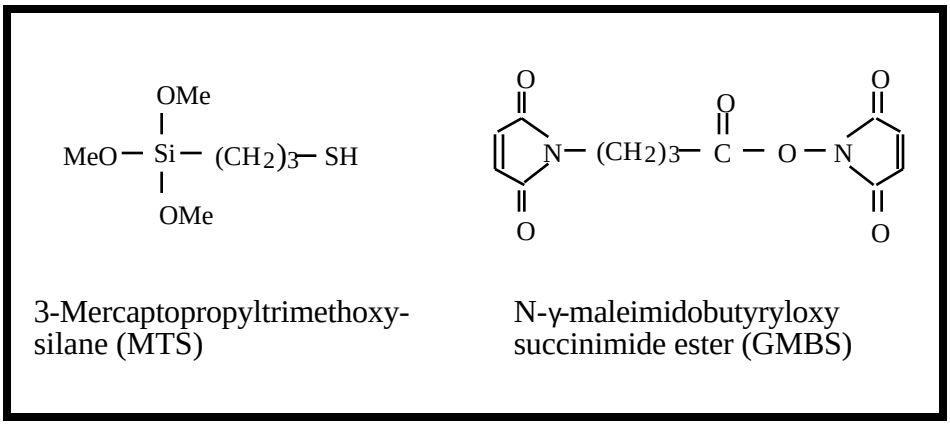

Figure 23: Silane and crosslinker used to covalently bind antibody to glass. [4]

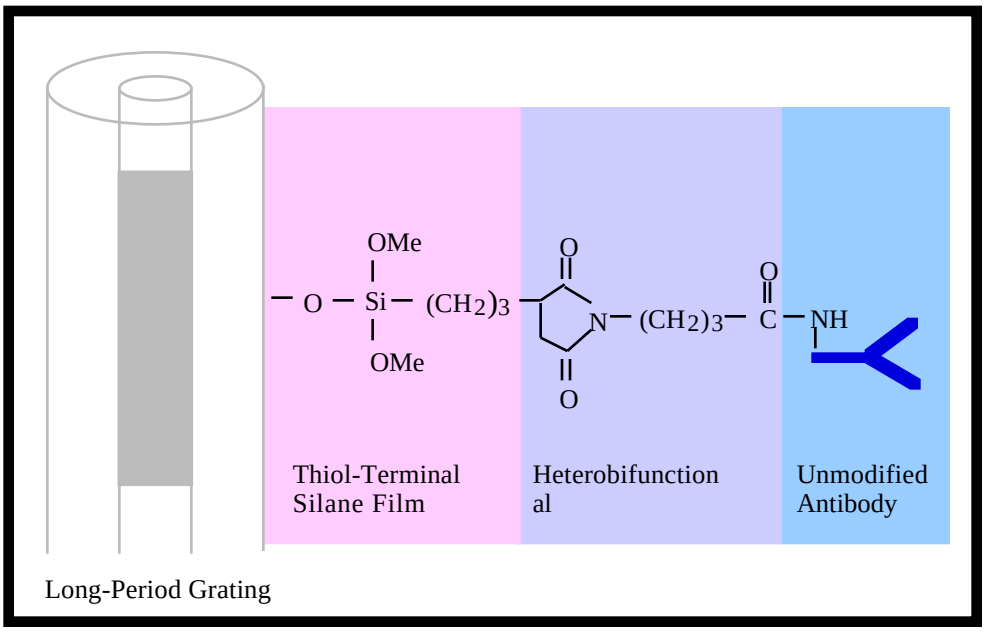

Figure 24: Summary of the silane-crosslinker procedure. [4]

5.0 EXPERIMENTAL

This chapter outlines several different attempts to make a viable biosensor from long-period gratings. Various techniques and procedures were used until reasonable results were obtained. The results are presented in tabular and graphical form. A short synopsis is given at the end of this chapter.

5.1 INITIAL EXPERIMENTS

Early experiments yielded marginal results. This section explains the problems associated with each trial and outlines attempts to increase the sensitivity of the sensor.

5.1.1 PREPARATION

The first gratings researched were written in AT&T dispersion shifted fibers with periods of hundreds of microns. After fabrication, the LPG's were tested in index oils and sucrose solutions to assess the gratings' refractive index sensitivity. Figure 25 shows the test set-up. As long-period gratings couple light into the cladding, the gratings are very bend sensitive. Two fiber holders clamp the grating firmly to prevent erroneous readings or overall attenuation. An adjustable stand raises a microscope slide to within a millimeter of the stripped fiber surface. The distance is maintained to prevent a response due to interaction with the glass surface of the slide. A test solution is applied, and the surface tension of the solution ensures the grating is completely enveloped. The spectrum is monitored with a light source and optical spectrum analyzer with a resolution of 0.2 nm.

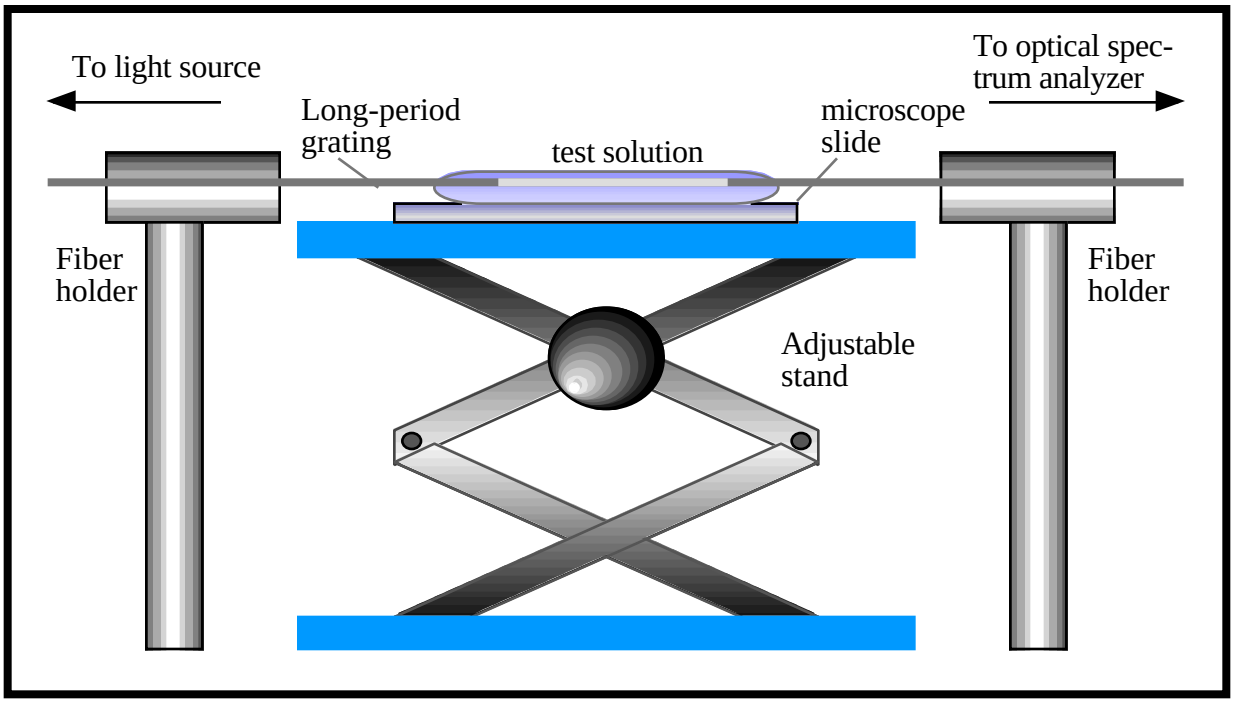

Figure 25: Experimental set-up for refractive index sensitivity tests.

The index of the oils ranged from 1.404 to 1.800 with a variance of ±0.0002. Figure 26 and Table 2 give the results of the index tests for a representative dispersion shifted fiber long-period grating. The LPG's showed significant index sensitivity only in a limited range of indices.

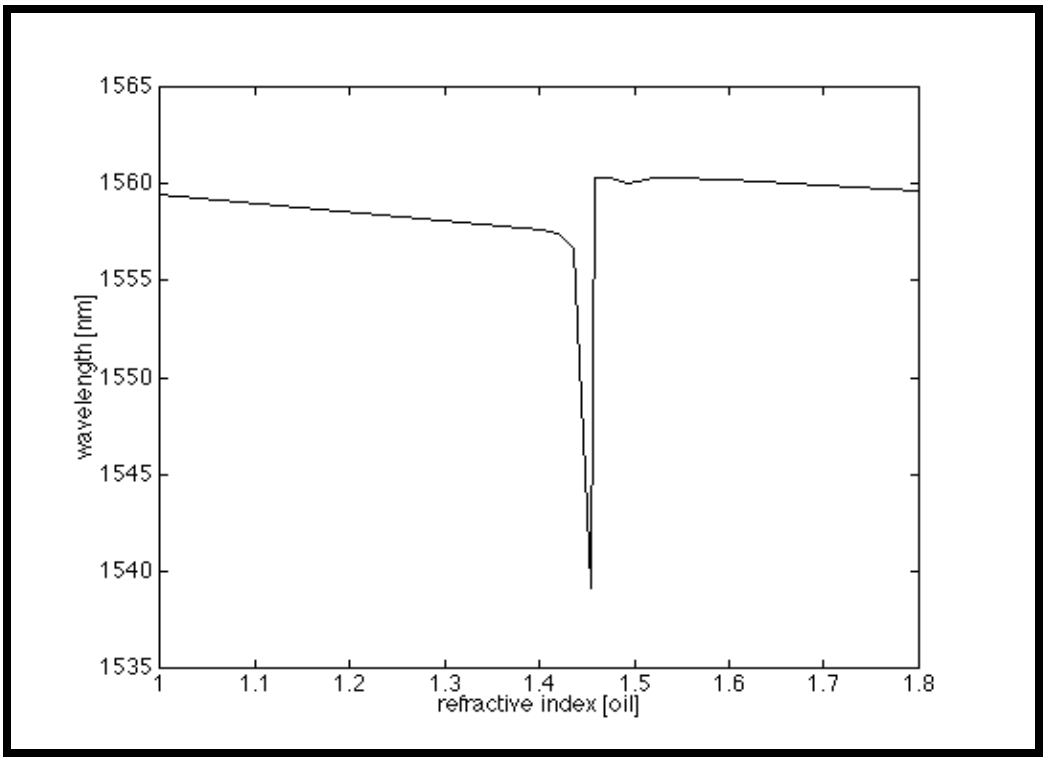

Figure 26: Index tests of dispersion shifted fiber long-period gratings with index oils.

refractive index	wavelength (nm)	refractive index	wavelength (nm)
Air (~1.0)	1559.48	1.476	1560.34
1.404	1557.58	1.492	1560.00
1.420	1557.41	1.520	1560.34
1.436	1556.55	1.540	1560.34
1.454	1539.13	1.600	1560.17
1.458	1560.34	1.800	1559.65

Table 2: Numerical results of index tests of figure 26.

Sucrose solutions were made to test indices between 1.33 and 1.42. Readings from a refractometer gave the index of the sucrose solutions to within ±0.00005. Figure 27 and Table 3 give the results of the sucrose tests for a representative grating. It was determined that there was no sensitivity in this region.

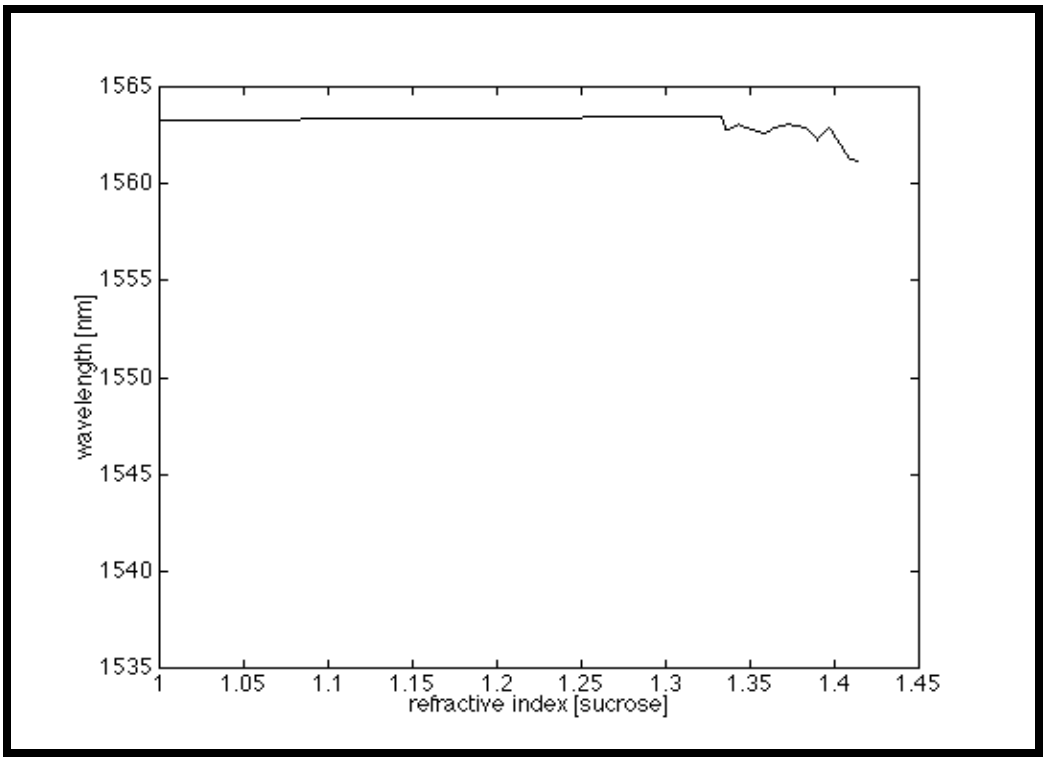

Figure 27: Index tests of dispersion shifted fiber long-period gratings with sucrose solutions.

refractive index	wavelength (nm)	refractive index	wavelength (nm)
Air (~1.0)	1563.27	1.3638	1562.93
1.3332	1563.44	1.3726	1563.10
1.3348	1562.75	1.3834	1562.93
1.3386	1562.93	1.3899	1562.24
1.3432	1563.10	1.3962	1562.93
1.3474	1562.93	1.4083	1561.37
1.3582	1562.58	1.4136	1561.20

Table 3: Numerical results of index tests of figure 27.

5.1.2 RESULTS OF THE COATING PROCEDURE

After testing with the refractive index solutions, the gratings were then coated according to the silane-crosslinker procedure. The spectrum of each grating was monitored before and after the

addition of antigen. Results showed marginal success. Shifts of two nanometers were observed indicating one of three possibilities: 1.) the antigen-antibody interaction did not produce desirably large index changes, 2.) the interaction occurred at an index outside the sensitive range of the grating, 3.) the coating procedure was not working as efficiently as anticipated.

The sensitivity of the grating was approximated as the change in index divided by the wavelength shift at that index range multiplied by the maximum resolution of the optical spectrum analyzer (OSA). For the grating of Figure 26, the sensitivity is 10^{-5} with an OSA resolution of 0.01 nm for a range of indices between 1.436 and 1.454. Even greater sensitivities were seen with gratings tested from AT&T Bell Laboratories. Other optical biosensors with the same or less index sensitivity were able to detect antigen-antibody interactions. It was determined that the interaction did produce sufficiently large index changes for the long-period gratings to detect.

To test the coating procedure, the experiment was attempted again with the spectrum monitored after each step: cleaning and hydroxylating, silanization, crosslinking, binding of antibody, and binding of antigen and blocking agent. Five gratings were fabricated and tested with the oils and sucrose solutions, then coated with the silane and crosslinker. Only one grating survived as structural stability was a severe problem in the beginning. The grating showed a three nanometer shift from cleaning to coating with silane. The observed shift disappeared with the addition of the crosslinker. The grating broke before the antibody could be applied. The results suggested that the crosslinking procedure displaced the silane from the glass surface or pushed the index of the layers beyond grating sensitivity.

With only one grating to provide data, it was difficult to make any sound conclusions. The early fabrication process required hours to produce each long-period grating until the facility was finalized as described in section 4.1. Reproduction of the experiment was to be delayed until other tests of the coating procedure had been exhausted. Plain fibers with the same dimensions as the gratings were stripped and coated with the silane and crosslinker. The fibers were then broken into small pieces for an ELISA test. The sandwich assay was performed with inconclusive results [3]. As the chemically induced color change phenomenon of the assay is immobilized onto the fiber in

a sandwich assay, a comparison to a gradient of aqueous solutions (as described in section 2.2.2) provides little insight. A second assay was attempted which leaves the color change in solution [3]. The second assay was unsuccessful, however, as the monolayers deposited onto the fiber interfered with the test [3].

5.1.3 ATTEMPTS TO IMPROVE SENSITIVITY

A dextran-hydrogel coating procedure was tried next in lieu of the silane and crosslinker. It promised more antibody binding capacity though the binding mechanism was adsorption [9]. The research also indicated that the index of the hydrogel could be adjusted to the sensitive region of the grating [3]. Details of the procedure can be found in section 4.2.1. The fiber gratings did not respond to the treatments, and ELISA assays proved just as uninformative as they had for the silane-crosslinking procedure. The dextran-hydrogel coatings were discontinued as the procedure took four days to complete and the adsorption binding mechanism did not allow reusability of the sensor.

Early attempts were made to adjust the sensitivity range of the long-period grating. Changing the effective index of the cladding would translate the gratings' most sensitive index ranges. Doping the cladding was considered, but the expense did not justify the minimal influence it would have. Etching the cladding was a more attractive option. AT&T dispersion shifted fibers were etched by immersion in hydrofluoric acid. The fiber diameter was measured using a laser micrometer, and index sensitivity was tested with index oils. Etching the cladding from an initial diameter of 125 μm to a final diameter of 100 μm improved the grating's sensitivity four fold [17]. The resonance condition and the most sensitive region occurred at slightly lower indices as the thinner cladding produced a smaller effective index [17]. The range of index sensitivity was also expanded as the reduced size of the cladding allowed more of the evanescent field to react with the outside medium [17]. The drawback to LPG etching was the further compromise of grating strength. As structural stability was already a problem, the etched gratings were not tested with the monolayer coatings.

At this point, several goals were set. Grating fabrication needed to become faster and more

At this point, several goals were set. Grating fabrication needed to become faster and more automatic. The facility described in section 4.1 was developed to allow writing of long-period gratings in approximately twenty minutes as opposed to several hours. The sensitivity and range of index sensitivity of the LPG's needed to be improved. Finally, structural stability needed to be addressed.

5.2 FINAL RESULTS

This section reports on the results of the final experiments. Proof of principle was accomplished after sensitivity and strength issues were resolved.

5.2.1 FABRICATION

After the fabrication facility was improved, long-period gratings could be written within twenty minutes. AT&T dispersion shifted fibers, Corning SMF-28 single-mode fibers, and Corning Flexcor 1060 fibers were converted to gratings and tested with index oils. The Corning Flexcor fibers were chosen for their high germanium content, ease of writing and analysis, and high index sensitivities. By using smaller periods and operating on inflection points of the characteristic curves for this fiber, index sensitivities and sensitivity ranges were improved (section 3.3). Coupling into high order cladding modes increases the power in the side lobes of the mode allowing more of the evanescent field to react with the ambient medium. High order cladding modes also see a smaller effective cladding index than their low order counterparts, giving rise to resonance conditions at lower indices.

To preserve the structural integrity of the grating during manufacturing and annealing, several stripping techniques were tried. The jacket of the fiber has to be removed to prevent it from melting onto the amplitude mask during irradiation of the core and to prevent any undesirable chemical interaction with the coating process. The former method of jacket removal was to strip the acrylate

the acrylate coating with a sharp razor. The edge of the razor runs along the length of the cladding, possibly scratching the glass and weakening it. To avoid damaging the cladding, immersion in a hot bath of 95% sulfuric acid and 5% nitric acid was tested. The hot acid bath renders the grating more sturdy than the former razor stripping technique. The best method of jacket removal, though, is immersion in methylene chloride. The jacket is nicked to allow the solution to penetrate before being submerged in a room temperature bath of methylene chloride. The solution strips the coating within two minutes after which the bared glass surface is rinsed in acetone. Gratings stripped in this manner retained the most strength.

Sixteen Corning Flexcor fibers were stripped by immersion in methylene chloride. The fibers were then converted to long-period gratings using the fabrication facility outlined in section 4.1. Each fiber was subjected to 120 - 140 mW of ultra-violet optical power. The gratings were written in fifteen minutes and reached a length of 1.5 cm. Periods ranged from 40 μm to 200 μm. The gratings were annealed at 130°C for fourteen hours. For identification purposes, each grating was given a designation code describing the number of the grating (1 - 16), the type of fiber the grating was written into (FLX for Corning Flexcor), and the period of the grating in microns. The following gratings were constructed for biosensor testing:

1/FLX/40	5/FLX/80	8/FLX/120	11/FLX/160	14/FLX/200
2/FLX/40	6/FLX/80	9/FLX/120	12/FLX/160	15/FLX/200
3/FLX/40	7/FLX/80	10/FLX/120	13/FLX/160	16/FLX/200.
4/FLX/40				

5.2.2 PREPARATION

After fabrication and annealing, the gratings were tested with index oils according the set-up shown in Figure 25 of section 5.1.1. Only six oils were used for the test as grating behavior is well known. Untested ranges can be approximated with data previously collected on similar gratings. Water was also used to represent an index of 1.33.

Figures 28 - 32 and Tables 4 - 8 show the data obtained from the index sensitivity tests. Several loss bands were monitored with each grating. The figures show the results from a representative grating for each period grouping. In the graphs, zero values represent the resonance condition where the loss band disappears. The index values 1.6 and 1.7 were added for a more intuitive appearance in each plot. The tables show the actual data collected for all of the monitored modes and gratings. The wavelength shifts are measured from the loss bands' original spectral position in air. A "~~" symbol corresponds to the resonance condition, and a "**" means that the loss band shifted beyond the range of the broadband light source. In Figure 30, zero values are substituted into the plot when the loss band goes beyond the source's band edge.

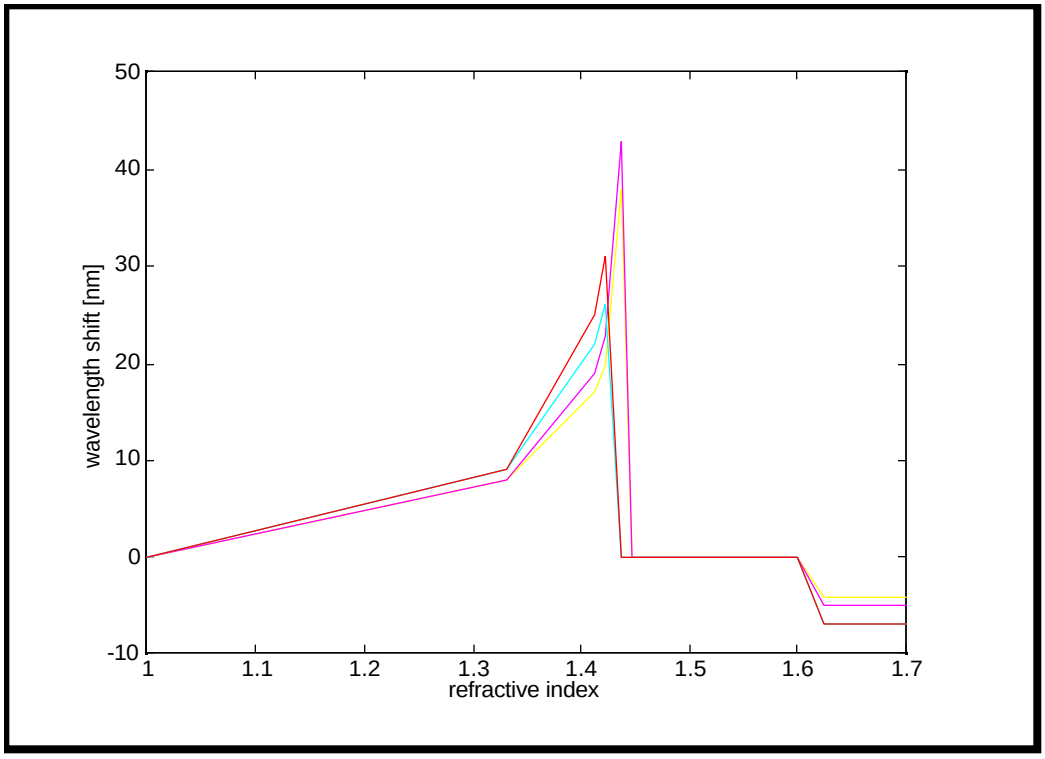

Figure 28: Graphical representation of index sensitivity test for grating 2/FLX/40. Four modes are depicted under the anomalous operating region.

INDEX:	1.33	1.412	1.420	1.436	1.448	1.454	1.624
1/FLX/40							
$\Delta\lambda_1$:	6	16	20	39	~~	~~	-6
$\Delta\lambda_2$:	7	18	22	~~	~~	~~	-6
$\Delta\lambda_3$:	8	22	27	~~	~~	~~	-6
2/FLX/40							
$\Delta\lambda_1$:	8	17	20	38	~~	~~	-4
$\Delta\lambda_2$:	8	19	23	43	~~	~~	-5
$\Delta\lambda_3$:	9	22	26	~~	~~	~~	-7
$\Delta\lambda_4$:	9	25	31	~~	~~	~~	-7
3/FLX/40							
$\Delta\lambda_1$:	6	16	18	34	~~	~~	-10
$\Delta\lambda_2$:	6	17	20	36	~~	~~	-10
$\Delta\lambda_3$:	7	22	24	~~	~~	~~	-10
$\Delta\lambda_4$:	6	24	30	~~	~~	~~	~~
4/FLX/40							
$\Delta\lambda_1$:	2	11	14	31	~~	~~	-9
$\Delta\lambda_2$:	4	14	17	36	~~	~~	-8
$\Delta\lambda_3$:	4	16	20	~~	~~	~~	-12
$\Delta\lambda_4$:	6	22	30	~~	~~	~~	~~

Table 4: Results of index sensitivity testing on 40 μm gratings written in Corning Flexcor fiber.

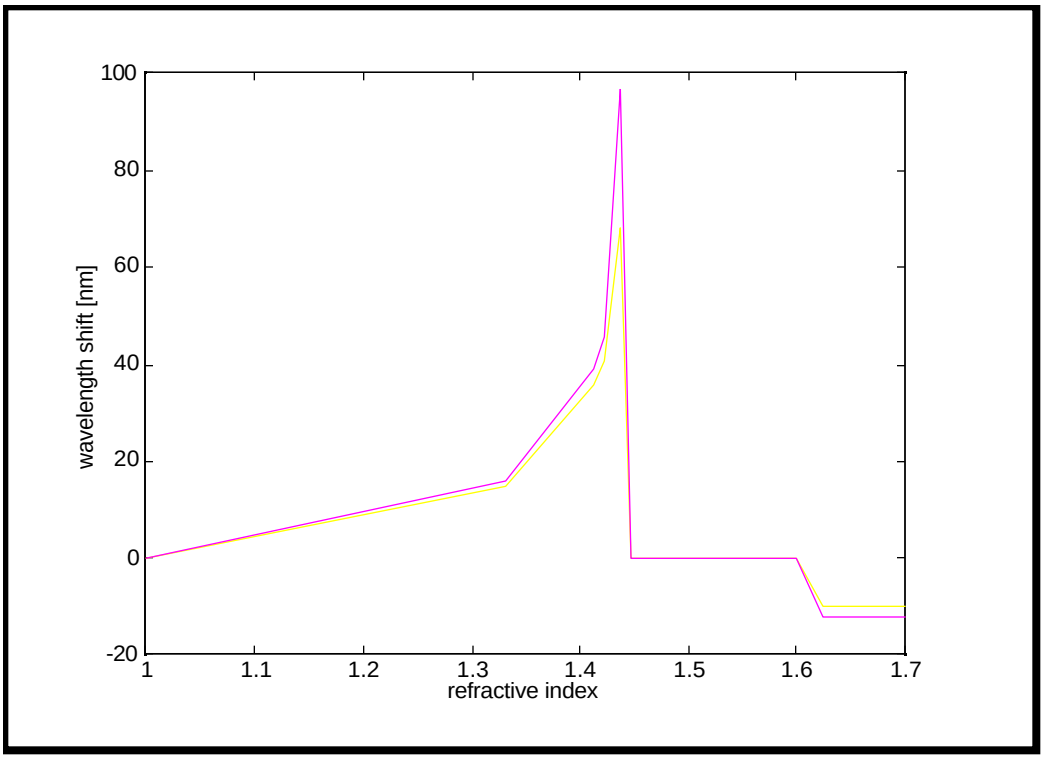

Figure 29: Graphical representation of index sensitivity test for grating 6/FLX/80. Two modes are depicted under the anomalous operating region.

INDEX:	1.33	1.412	1.420	1.436	1.448	1.454	1.624
5/FLX/80							
$\Delta\lambda_1$:	14	35	40	67	~~	~~	-11
$\Delta\lambda_2$:	13	37	44	94	~~	~~	-16
6/FLX/80							
$\Delta\lambda_1$:	15	36	41	68	~~	~~	-10
$\Delta\lambda_2$:	16	39	46	97	~~	~~	-12
7/FLX/80							
$\Delta\lambda_1$:	15	34	41	64	~~	~~	-14
$\Delta\lambda_2$:	15	37	45	90	~~	~~	-15

Table 5: Results of index sensitivity testing on 80 µm gratings written in Corning Flexcor fiber.

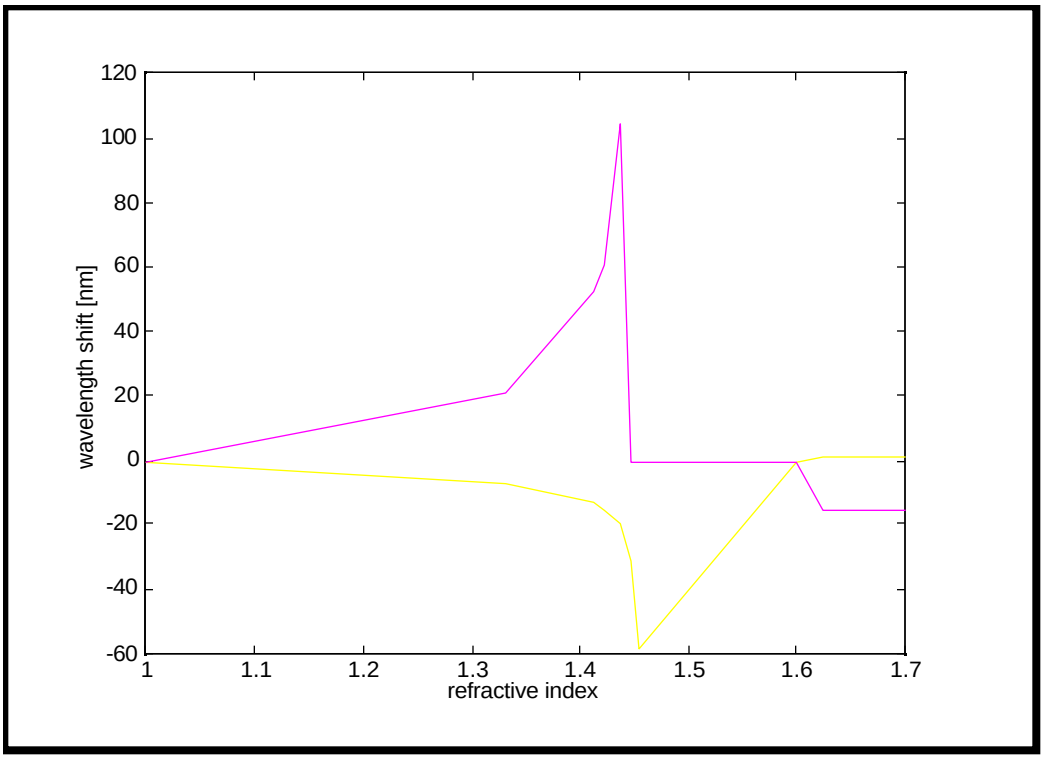

Figure 30: Graphical representation of index sensitivity test for grating 8/FLX/120. Two modes are depicted. The grating operates on an inflection curve in the λ vs Λ plot.

INDEX:	1.33	1.412	1.420	1.436	1.448	1.454	1.624
8/FLX/120							
$\Delta\lambda_1$:	-7	-13	-15	-19	-31	-58	1
$\Delta\lambda_2$:	21	53	61	105	**	**	-15
9/FLX/120							
$\Delta\lambda_1$:	-4	-10	-12	-16	-26	-49	3
$\Delta\lambda_2$:	19	50	60	103	**	**	-14
10/FLX/120							
$\Delta\lambda_1$:	-1	-8	-8	-13	-22	-44	7
$\Delta\lambda_2$:	11	49	57	103	**	**	-15

Table 6: Results of index sensitivity testing on 120 μm gratings written in Corning Flexcor fiber.

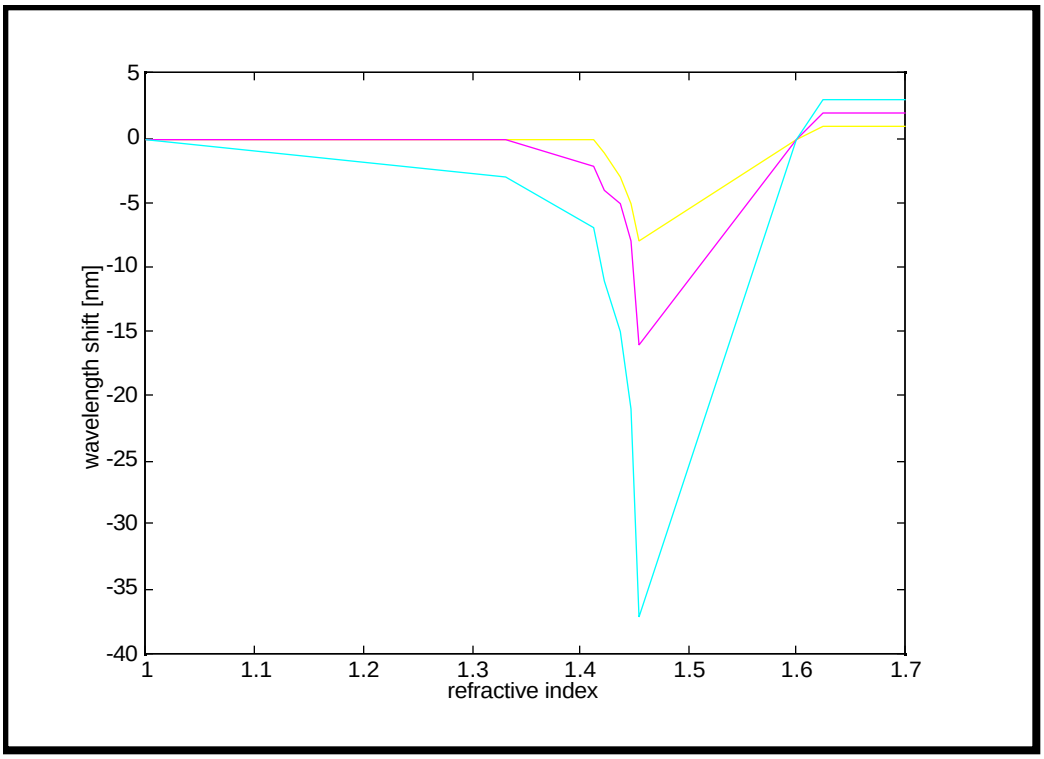

Figure 31: Graphical representation of index sensitivity test for grating 12/FLX/160. Three modes are depicted in normal grating operation.

INDEX:	1.33	1.412	1.420	1.436	1.448	1.454	1.624
11/FLX/160							
$\Delta\lambda_1$:	-1	-2	-2	-3	-5	-8	1
$\Delta\lambda_2$:	0	-2	-3	-4	-7	-13	2
$\Delta\lambda_3$:	-1	-7	-7	-11	-18	-34	4
12/FLX/160							
$\Delta\lambda_1$:	0	0	-1	-3	-5	-8	1
$\Delta\lambda_2$:	0	-2	-4	-5	-8	-16	2
$\Delta\lambda_3$:	-3	-7	-11	-15	-21	-37	3
13/FLX/160							
$\Delta\lambda_1$:	0	-1	-2	-4	-5	-9	1
$\Delta\lambda_2$:	0	-2	-4	-6	-9	-17	2
$\Delta\lambda_3$:	-2	-7	-10	-13	-21	-41	4

Table 7: Results of index sensitivity testing on 160 µm gratings written in Corning Flexcor fiber.

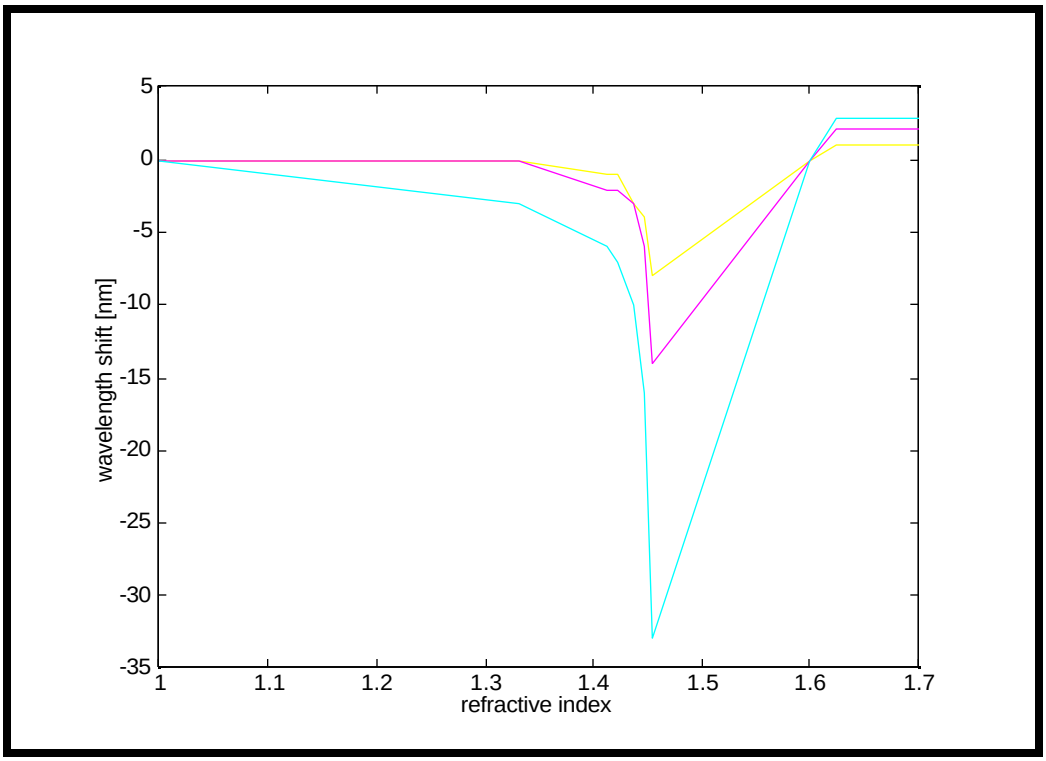

Figure 32: Graphical representation of index sensitivity test for grating 14/FLX/200. Three modes are depicted in normal grating operation.

INDEX:	1.33	1.412	1.420	1.436	1.448	1.454	1.624
14/FLX/200							
$\Delta\lambda_1$:	0	-1	-1	-3	-4	-8	1
$\Delta\lambda_2$:	0	-2	-2	-3	-6	-14	2
$\Delta\lambda_3$:	-3	-6	-7	-10	-16	-33	3
15/FLX/200							
$\Delta\lambda_1$:	0	-1	-3	-4	-6	-9	0
$\Delta\lambda_2$:	0	-2	-3	-5	-8	-13	1
$\Delta\lambda_3$:	-3	-6	-8	-11	-17	-31	3
16/FLX/200							
$\Delta\lambda_1$:	0	0	-1	-3	-4	-7	1
$\Delta\lambda_2$:	0	-2	-3	-5	-8	-14	1
$\Delta\lambda_3$:	-3	-6	-7	-10	-16	-30	3

Table 8: Results of index sensitivity testing on 200 µm gratings written in Corning Flexcor fiber.

5.2.3 COATING WITH SILANE AND CROSSLINKER

Figure 33 shows how the long-period gratings are coated with the various monolayers. Several configurations were tested from mounting each grating on a glass slide assembly to using unreactive, milled Teflon containers. The set-up shown in Figure 33 allows larger solution volumes to be applied while requiring the least amount of handling. The gratings are immersed in solutions contained by a glass petri dish. The dish can be changed after each step, ensuring that the entire coating procedure does not take place on the glass of the container. Use of a single volume of solution gives way to uniformly coated gratings which can be compared to one another. Consistent stirring and mixing is also facilitated with the single petri dish set-up. The individual gratings are held straight by hand when spectral output readings are taken.

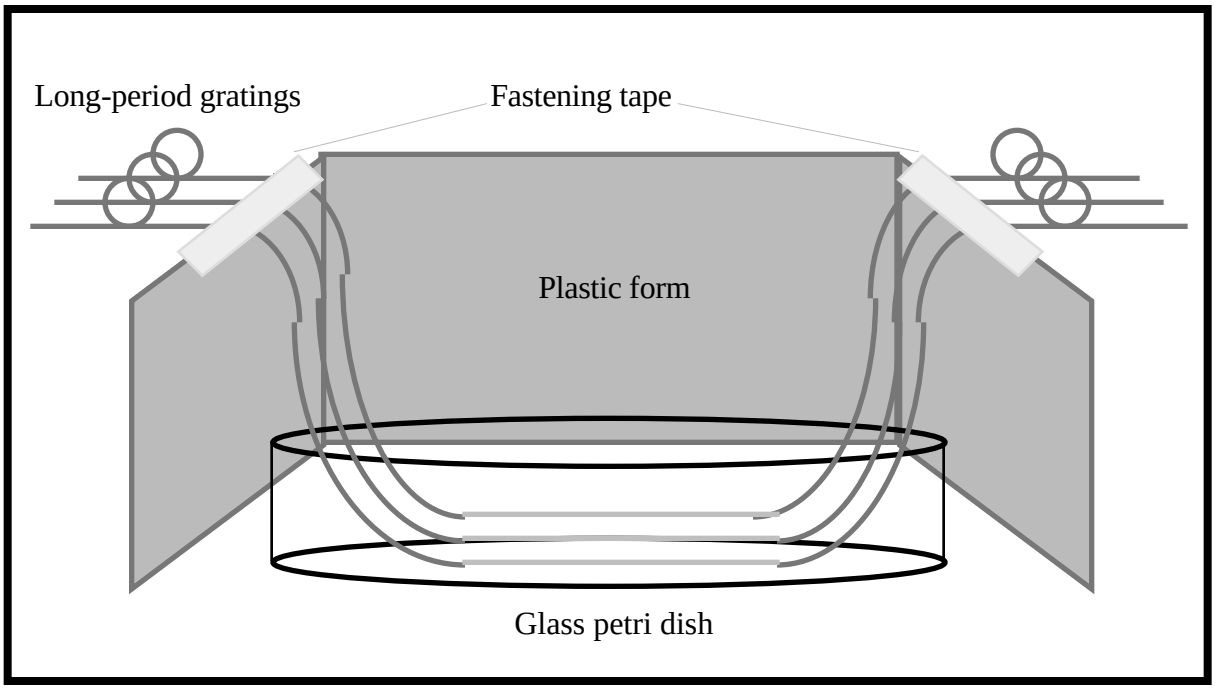

Figure 33: Experimental set-up for monolayer coating procedure.

The first step in the coating procedure is cleaning and hydroxylating the cladding surface. The gratings are immersed sequentially in a 1:1 mixture of hydrochloric acid and methanol, sulfuric acid, and boiling distilled water [4]. Each of the three solutions is in contact with the glass for thirty

thirty minutes, then rinsed in distilled water [2]. The fibers are allowed to air dry until the next step [4].

The silane layer is applied with a 4% solution of 3-mercaptopropyltrimethoxysilane (MTS) (Aldrich, Milwaukee, WI) in anhydrous toluene (Aldrich) [2]. As the literature does not specify volume per volume (v/v) or weight per weight (w/w) ratios, both were calculated [2,4]. A 4% v/v solution corresponds to 4 mL of MTS in a total volume of 100 mL, thus permitting 96 mL of the anhydrous toluene. The w/w calculation was solved with the following equation:

$$4\%\ \text{w/w} := \frac{\text{vol MTS [mL] x dens MTS [g/mL]}}{\text{vol MTS [mL] x dens MTS [g/mL] + vol toluene [mL] x dens toluene [g/mL]}}, \qquad (5.1)$$

where vol is volume and dens is density. The density of MTS is 1.039 g/mL and that of the anhydrous toluene is 0.865 g/mL [18]. Solving equation (5.1) gives 3.35 mL of MTS with 96.65 mL of toluene for a total volume of 100 mL. To maximize the amount of silane available to the fibers, the 4% v/v interpretation was used.

The silane step must be carried out in an inert atmosphere [2,4]. The experiment is conducted in a glove box (donated by the Chemistry Department of Virginia Polytechnic Institute and State University) with a constant supply of purified nitrogen gas (Industrial Gas and Supply, Radford, VA). To preserve the purity of the toluene, Aldrich supplies the chemical under a nitrogen cap in a glass bottle secured with a rubber seal. The toluene is extracted with a syringe while nitrogen is injected with a second needle to balance the pressure. After the silane mixture is added to the gratings, the solution sits for thirty minutes [2]. The gratings are then rinsed in toluene and allowed to air dry [4].

The crosslinking step is the last step before antibody attachment. N-γ-maleimidobutyryloxy succinimide ester (GMBS) (Pierce, Rockford, IL) is dissolved in a minimum amount of dimethylformamide (DMF) (Aldrich) and diluted in absolute ethanol to a concentration of 2 mM (millimolar or 10^{-3} moles per liter). To determine the correct proportions of GMBS and ethanol, the following equation is used:

$$\text{volume ethanol [L]} := \frac{\text{mass of GMBS sample [g]}}{2 \times 10^{-3}\ \text{[mol/L]} \times \text{formula weight GMBS [g/mol]}} \quad . \qquad (5.2)$$

The formula weight of GMBS is 280.24 g/mol [1]. With a 50 mg sample of GMBS, 89.2 mL of ethanol is needed for a 2 mM solution. This solution is allowed to react with the silane on the fibers for one hour after which the gratings are washed in phosphate buffered silane (PBS) (Pierce) [2]. Again, the gratings are allowed to air dry [4].

To prevent excessive handling and breakage, only one grating from each period grouping was tested after each step of the coating procedure. Despite the precaution, gratings 1/FLX/40, 3/FLX/40, and 9/FLX/120 did break. Losing only three gratings in sixteen was a vast improvement over earlier attempts owing to the methylene chloride stripping technique and petri dish application method. Gratings 2/FLX/40, 5/FLX/80, 8/FLX/120, 11/FLX/160, and 14/FLX/200 were chosen for testing of the coating procedure. The results are summarized in Table 9 and Figures 34 - 38. The data was collected with an Ando optical spectrum analyzer using the high sensitivity setting and 2.0 nm resolution.

	Air	Silane	Xlinker	Antibody
2/FLX/40	845 945 1150 1260 1380	850 951 1158 1271 1385	850 951 1158 1269 1400	852 954 1160 1270 none
5/FLX/80	1208 1468	1222 1488	1228 none	1225 none
8/FLX/120	808 868 1548	807 867 1550	804 864 1554	808 866 1558
11/FLX/160	856 956	860 956	860 958	856 none
14/FLX/200	926 954 1138 1374	930 955 1134 1358	926 955 1136 1358	924 952 1134 1356

Table 9: Position of loss bands [nm] after each step of coating test. “None” means no loss band was detectable.

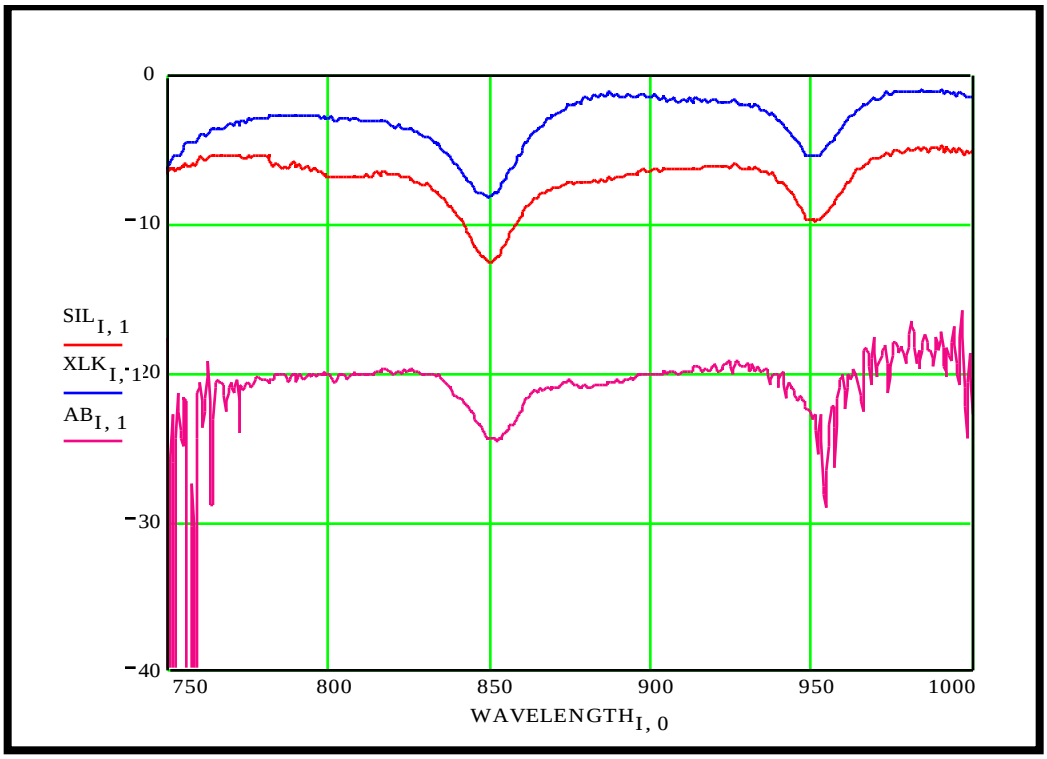

Figure 34: Spectral plots of coating test on 2/FLX/40 [dBm vs nm]. Initial plot in air is missing.

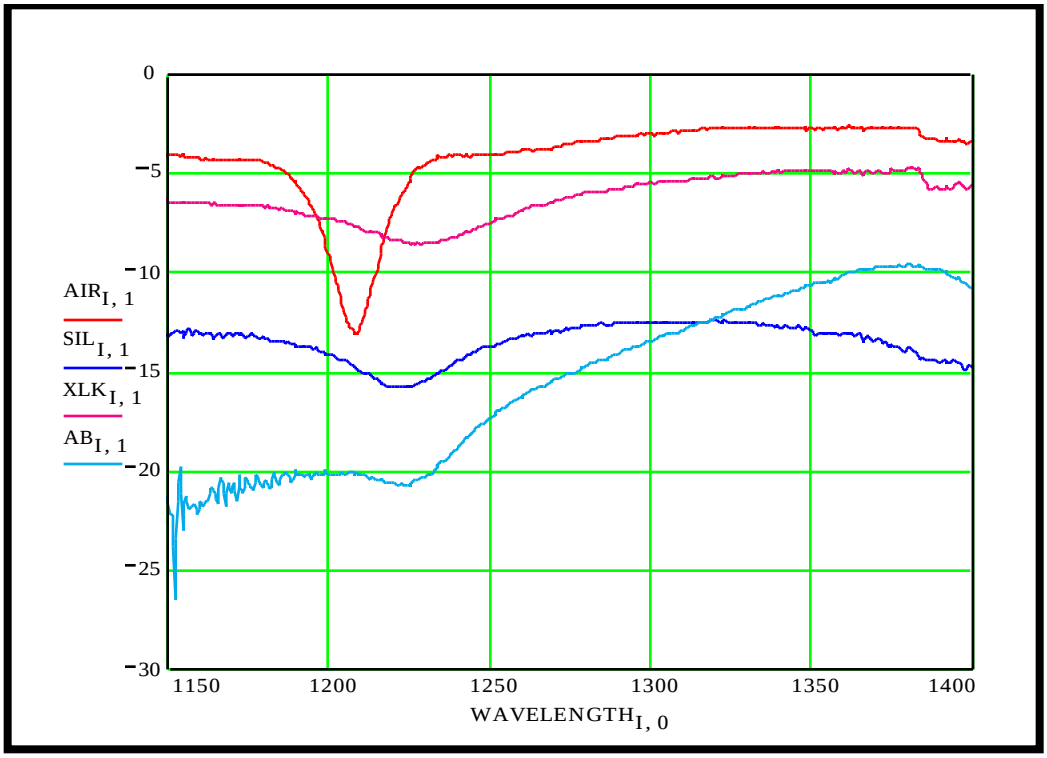

Figure 35: Spectral plots of coating test on 5/FLX/80 [dBm vs nm].

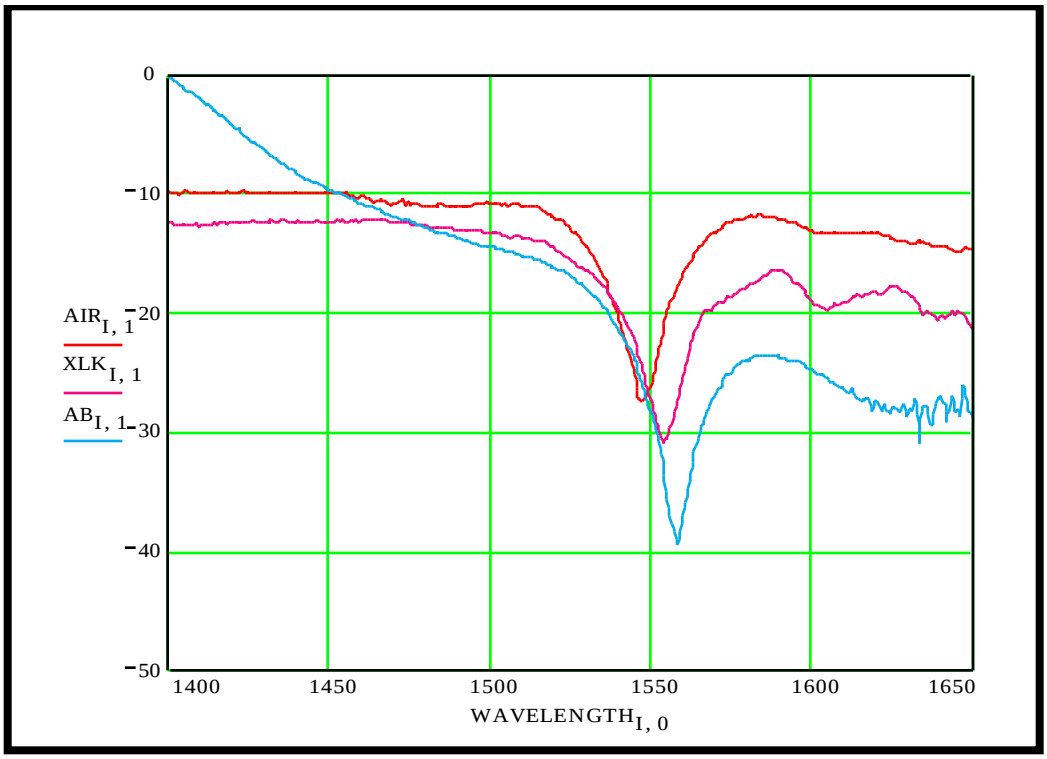

Figure 36: Spectral plots of coating test on 8/FLX/120 [dBm vs nm]. Silane plot is missing.

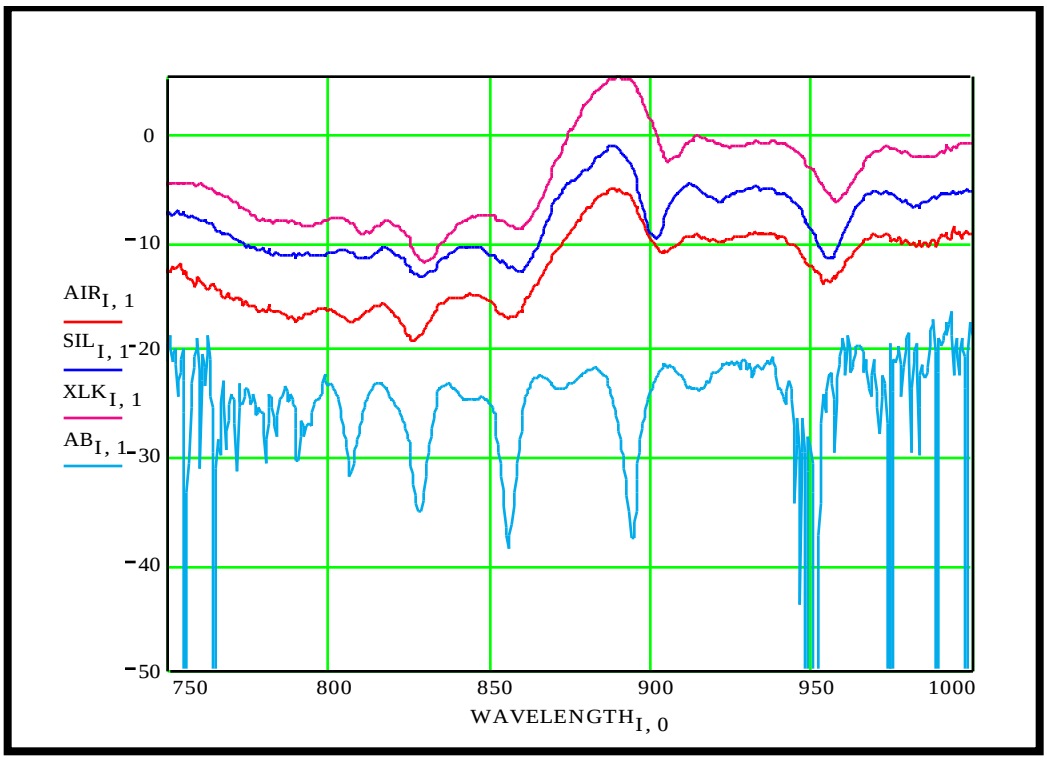

Figure 37: Spectral plots of coating test on 11/FLX/160 [dBm vs nm].

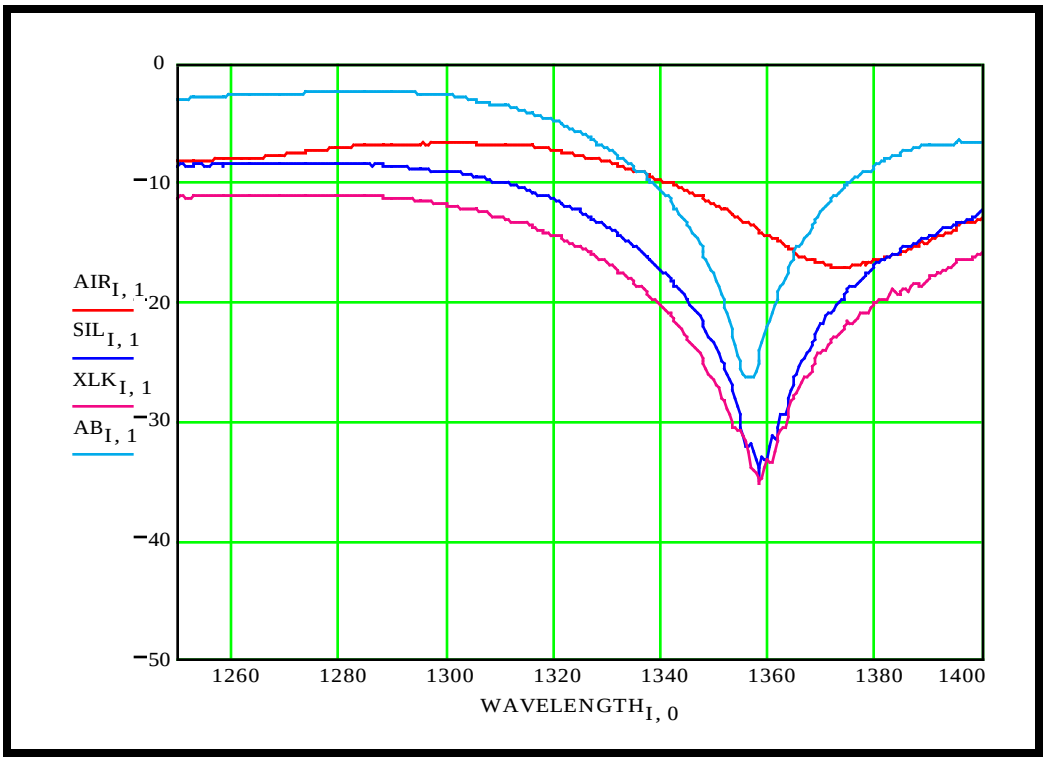

Figure 38: Spectral plots of coating test on 14/FLX/200 [dBm vs nm].

Though some of the modes of each grating experienced little change, the results show that a chemical interaction did take place. By comparison to the index tests of section 5.2.2, the silane deposit has an estimated index above 1.40, and the crosslinker layer increases that index to above 1.43. The silane with its heavy index and close proximity to the cladding gives rise to greater wavelength shifts than the crosslinker. Addition of antibody also has a small, but usually noticeable effect. The antibody and antigen applications are detailed in the next section.

5.2.4 ANTIGEN-ANTIBODY INTERACTION

Goat anti-human polyclonal affinity purified antibody (Pierce) was diluted in PBS to a concentration of 0.05 mg/mL and applied to the gratings for one hour [4]. After treatment, the gratings were washed in PBS to remove any antibody that was not covalently bound. The fibers were allowed to air dry before spectral output readings were taken.

The goat anti-human antibodies react with human immunoglobulin (IgG) but have a reduced cross-sensitivity to horse IgG [1]. The human IgG (Pierce) and horse IgG (Pierce) were both selected as antigen test solutions to analyze the specificity of the antigen binding. Gratings 4/FLX/40, 7/FLX/80, 10/FLX/120, 13/FLX/160, and 16/FLX/200 were separated from the rest for horse IgG application. The other surviving gratings were to be treated with the human IgG. A blocking agent of bovine serum albumen (BSA) (Pierce) was diluted in PBS to approximately 2 mg/mL and applied to both sets of gratings [4]. The blocking agent ensures that the antigen binds only through the antibody [4]. The antigen compounds were each diluted in PBS to 0.05 mg/mL and added separately to the BSA solutions [4]. The fibers incubated simultaneously for one hour before washing in PBS [4]. After excess antigen had been removed, the fibers were allowed to air dry and the spectral outputs were recorded.

Only the 80 μm, 120 μm, and 200 μm gratings showed any response to human IgG. None of the horse IgG treated gratings demonstrated antigen binding, as was expected. Table 10 summarizes the results of the antibody-antigen testing. Severely diminished loss bands corresponding to resonance conditions or loss bands which moved into the sources' noise regions are labeled as "none". Figures 39 - 47 show the recorded data of the spectrum analyzer operating on the high sensitivity setting with a resolution of 2.0 nm. The 80 μm, 120 μm, and 200 μm period grating groupings are shown for comparison purposes. The recorded data of the other gratings is left as an appendix.

	Air	Goat anti-human	Human IgG	Horse IgG
2/FLX/40	845 1150 1260	852 1160 1270	852 1156 1274	
4/FLX/40	842 1250	849 1268		850 1267
5/FLX/80	1208	1225	~1240	
6/FLX/80	1218	1224	1224	
7/FLX/80	1218	1226		1226
8/FLX/120	808 868 1548	808 866 1558	808 863 none	
10/FLX/120	852 1564	848 none		849 none
11/FLX/160	856	856	856	
12/FLX/160	902	901	900	
13/FLX/160	908	912		912
14/FLX/200	926 954 1138 1374	924 952 1134 1356	924 951 1138 1355	
15/FLX/200	952 1136 1372	952 1136 1364	950 1138 1354	
16/FLX/200	1132 1356	1128 1345		1128 1342

Table 10: Center wavelengths of loss bands [nm] for the antibody-antigen tests.

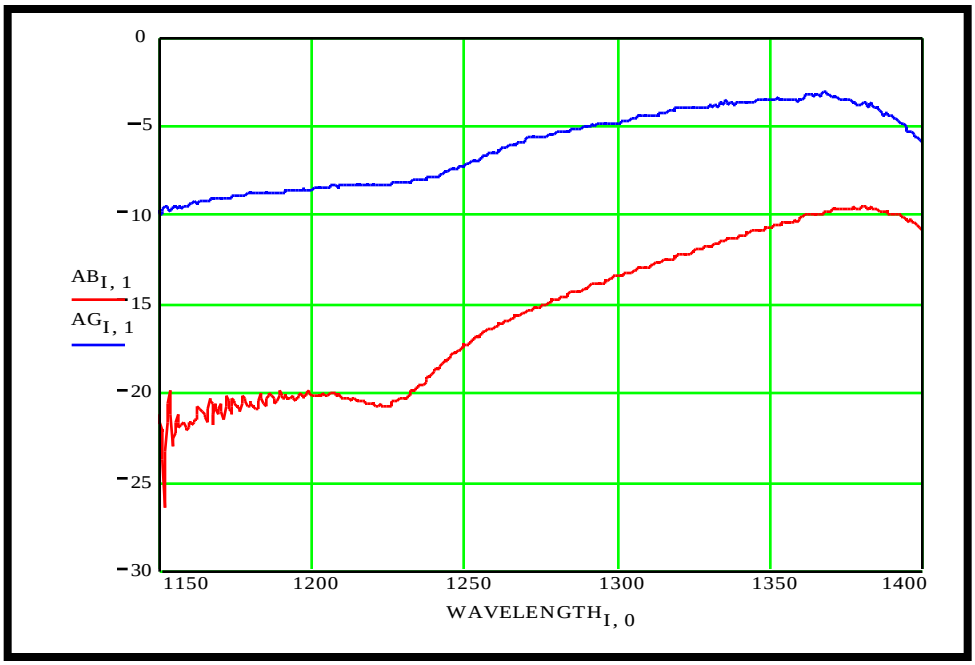

Figure 39: Antibody-antigen test for grating 5/FLX/80 with goat anti-human IgG and human IgG.

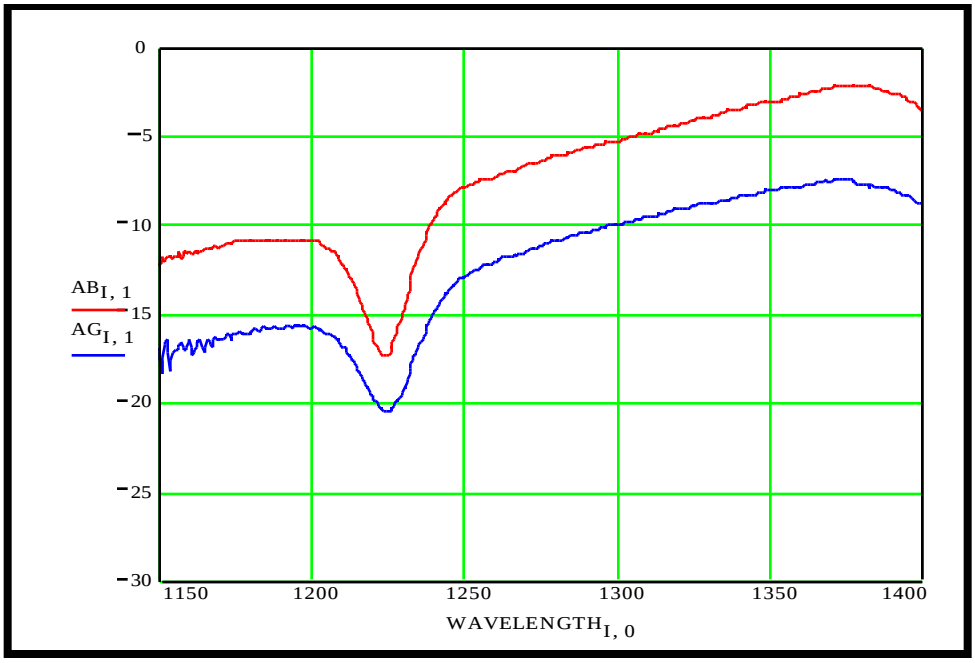

Figure 40: Antibody-antigen test for grating 6/FLX/80 with goat anti-human IgG and human IgG.

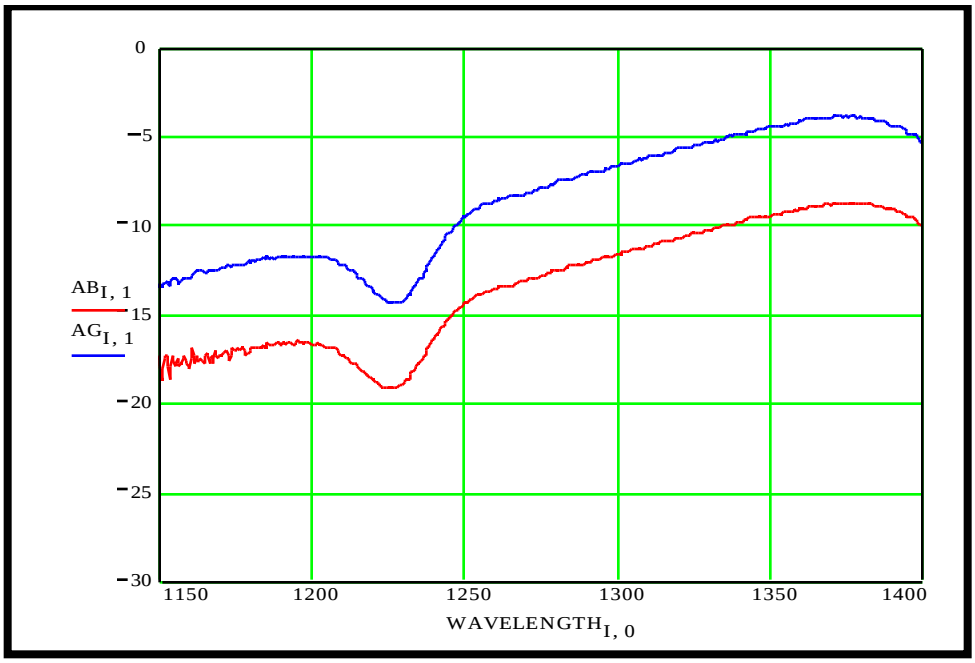

Figure 41: Antibody-antigen test for grating 7/FLX/80 with goat anti-human IgG and horse IgG.

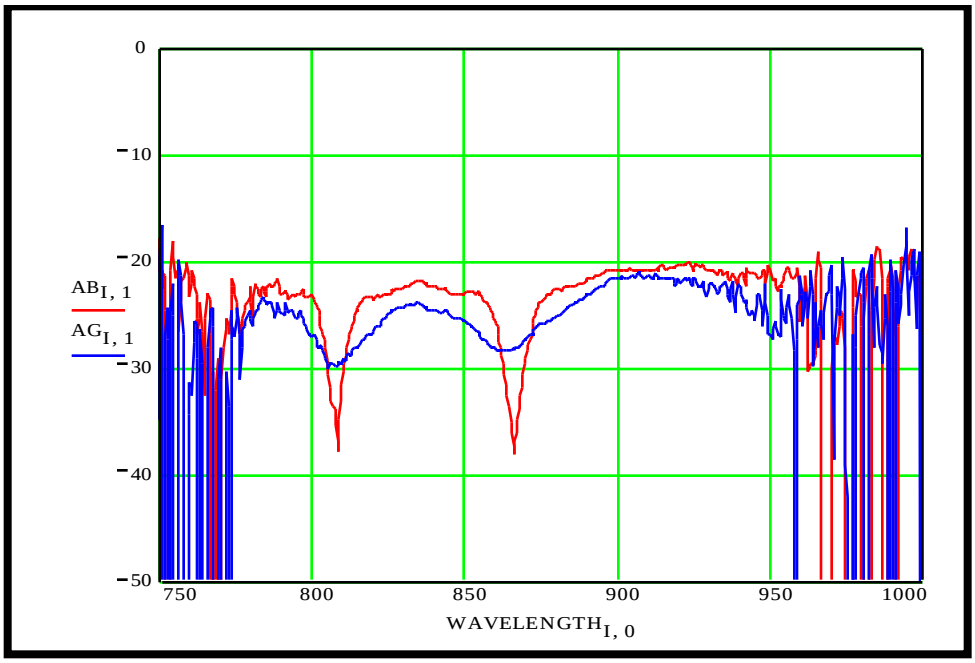

Figure 42: Antibody-antigen test for grating 8/FLX/120 with goat anti-human IgG and human IgG.

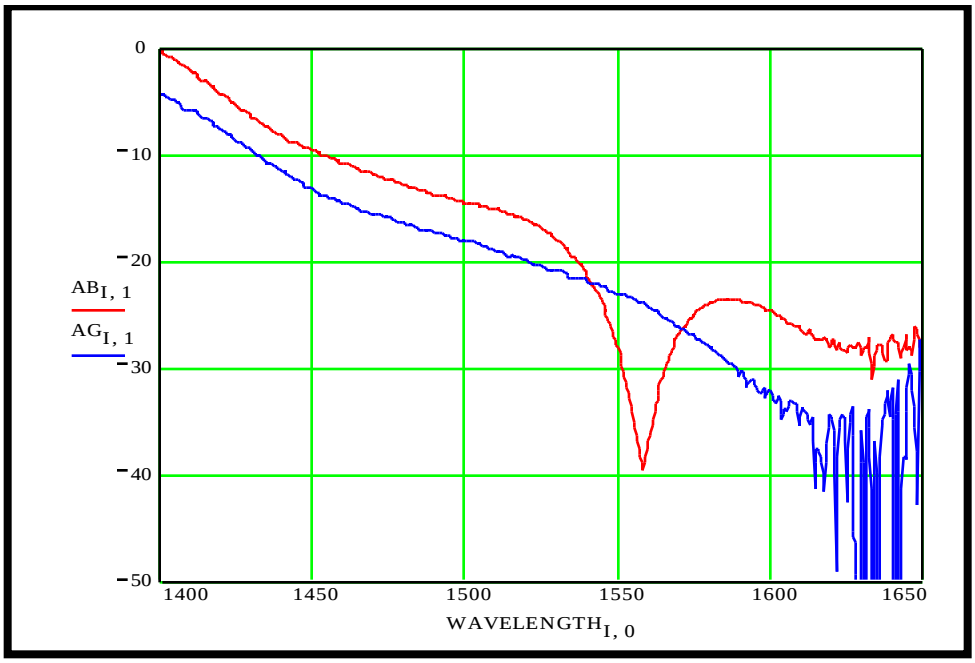

Figure 43: Antibody-antigen test for grating 8/FLX/120 with goat anti-human IgG and human IgG.

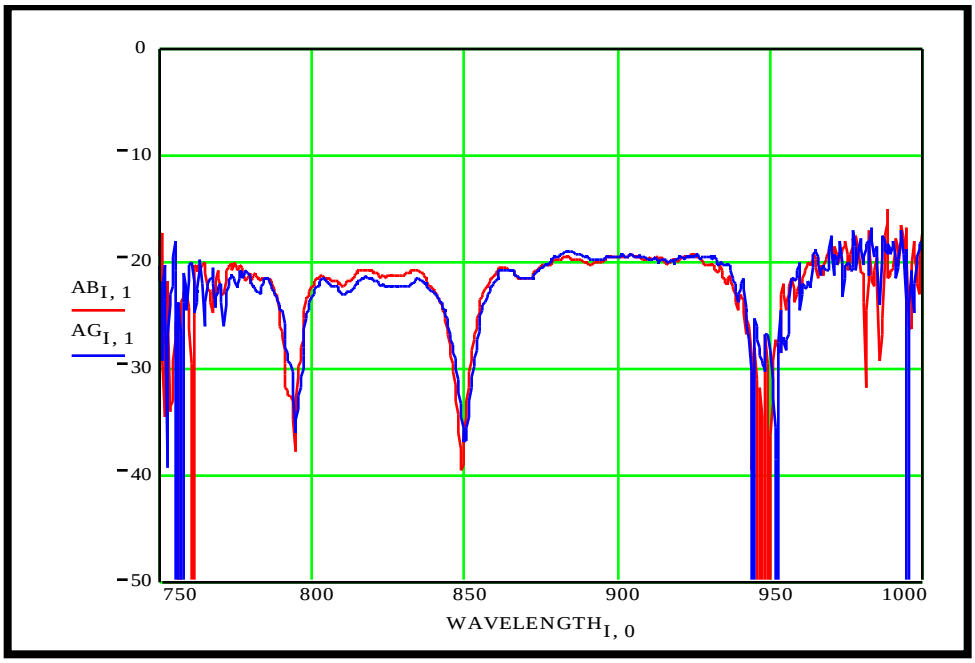

Figure 44: Antibody-antigen test for grating 10/FLX/120 with goat anti-human IgG and horse IgG.

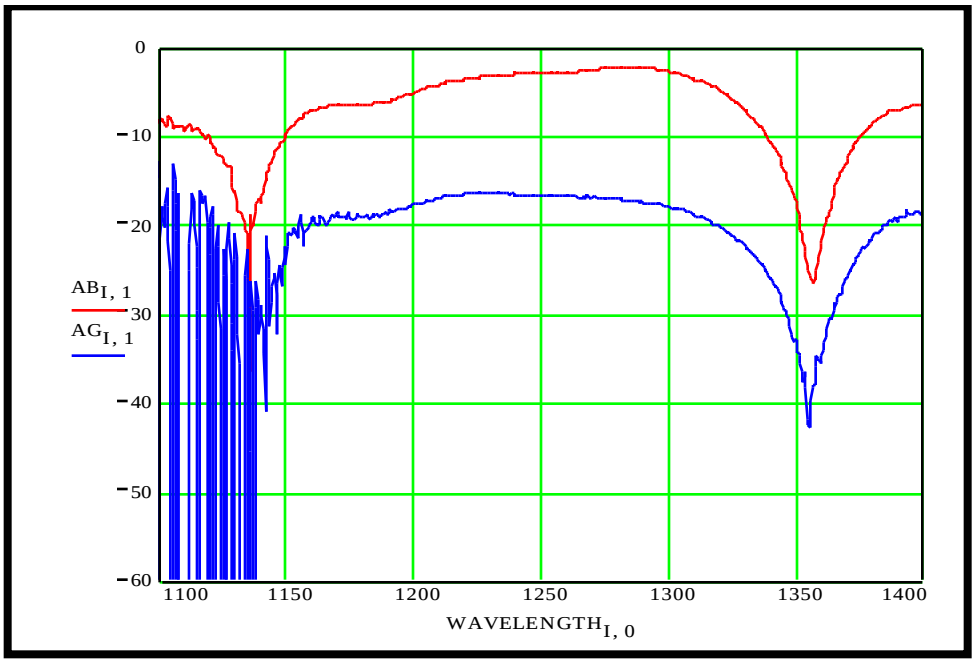

Figure 45: Antibody-antigen test for grating 14/FLX/200 with goat anti-human IgG and human IgG.

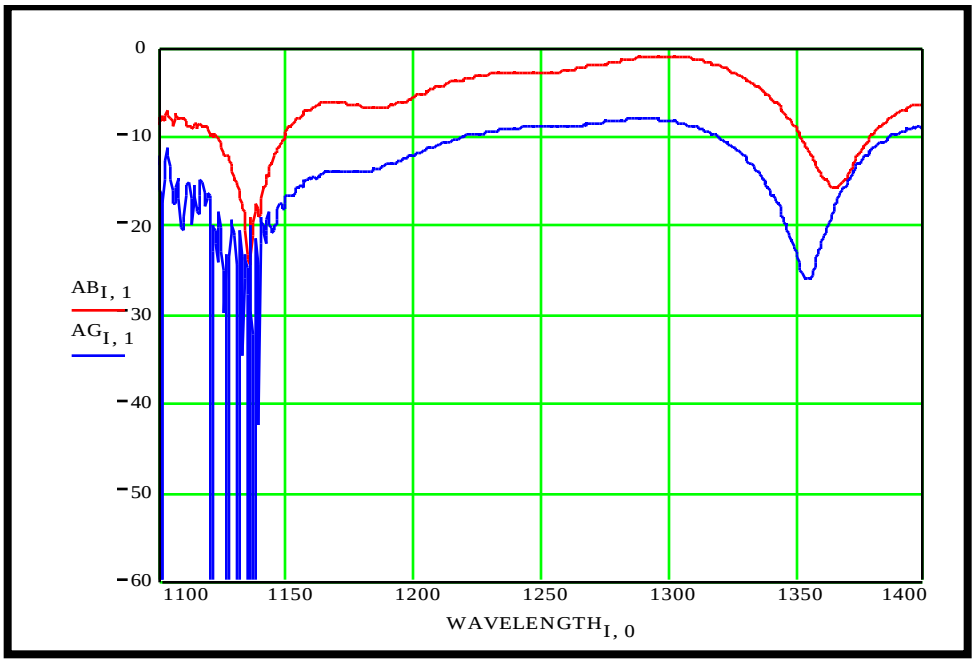

Figure 46: Antibody-antigen test for grating 15/FLX/200 with goat anti-human IgG and human IgG.

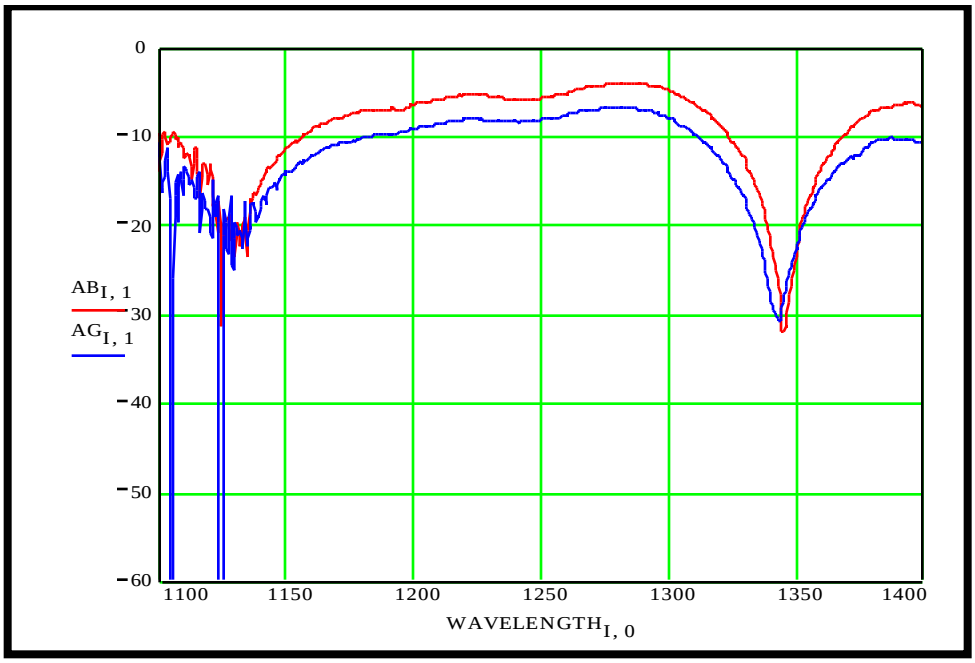

Figure 47: Antibody-antigen test for grating 16/FLX/200 with goat anti-human IgG and horse IgG.

The results demonstrated by Table 10 clearly show that the surface of the gratings did undergo a chemical reaction from the cleaning step to the application of antibody. The lack of response of the horse IgG treated gratings can not be attributed to the absence of silane, crosslinker, and antibody. Of the spectral responses shown in Figures 39 - 47, the 80 μm period grouping proved the least responsive. Grating 8/FLX/120 displayed an absence of the loss band when human IgG was applied. The loss band disappearance suggests that the isolation moved more than 50 nm into the noise region, as this particular mode moves to higher wavelengths with an increase in the effective cladding index. Unfortunately, the isolation of grating 10/FLX/120 experienced the same phenomenon before the antibody was applied. The horse IgG treated 10/FLX/120 could not be compared to the human IgG treated 8/FLX/120 in the 1100 - 1400 nm region.

Grating 15/FLX/200 experienced a 10 nm shift with the application of human IgG, whereas its 16/FLX/200 horse IgG counterpart showed only a 3 nm shift. The small shift of the latter grating can be attributed to the blocking agent, giving the 15/FLX/200 a decisive 7 nm shift over the horse IgG treated grating. Grating 14/FLX/200, which was also treated with human IgG, showed no response to the antigen. One explanation could come from Table 10. The table shows a 20 nm

shift from air to antibody for 14/FLX/200 as opposed to a 10 nm shift for the 15/FLX/200 and 16/FLX/200 gratings. The difference in responses to the coating procedure suggest that the 14/FLX/200 grating may not have been coated as uniformly as expected. The variance can be attributed to excessive handling when the grating was monitored after each step of the coating procedure. In addition, the grating did experience difficulties with its jacket which caused the bare part of the fiber to get tangled rather often during the experiment.

5.3 SYNOPSIS

The use of different cladding modes increased the sensitivity and range of the biosensor. The silane-crosslinker procedure was able to covalently bind antibody onto the glass surface of the grating with specific antigen binding capacity. The coating process also allowed the antigen-antibody interaction to take place within the sensitive range of most of the gratings. The 40μm and 160 μm gratings did not exhibit substantial antigen response.

Two final considerations of the interpretation of the results must be addressed. As the gratings were each straightened by hand during OSA scans with minimal force, strain response is considered negligible. Significant strain responses (more than one nanometer) are only seen with mechanical stretching or noticeable human effort. In addition, care was taken to perform the antibody and antigen tests on the same day so that temperature fluctuations within the lab could be ignored. Temperatures would need to vary by more than 10°C for any significant temperature response interference [14]. Such a variation was never encountered.

6.0 CONCLUSIONS AND FUTURE DIRECTIONS

A unique biosensor was created by combining biochemistry with the electromagnetics of long-period gratings. The sensor does not require a second layer of antibodies or the labeling of biochemical reagents to function. The covalent binding scheme utilized allows reusability of the device. Real-time analysis within a short period of time is possible with a minimum of detection equipment. Sensor fabrication is fast and simple. Structural stability has been improved with the aid of methylene chloride stripping techniques. Finally, the use of fiber optics allows remote sensing capabilities from the detection apparatus.

The minimum threshold of antigen detection should be investigated. ELISA tests on antigen solutions before and after application to the gratings would aid in determining resolution. Flow chambers for each coating step and for the addition of antibody and antigen has the potential of increasing sensitivity. Gratings written with periods of smaller increments than those demonstrated between 120 μm and 200 μm would better characterize which modes respond best to the antigen-antibody interaction. Finally, upgrading the available equipment to high precision instruments and developing better handling techniques during testing would aid in sensor evaluation.

The biosensor which has been created has great potential for expanded applications. Numerous antibodies have been designed to detect foreign substances in mammalian tissue, blood, and excretions. The coating procedure outlined in this research requires a primary amine group on the analyte for the necessary covalent binding. Coating schemes can be developed to react with other functional groups of interest. Sensing can range from antibody-antigen interactions to the detection of important ionic substances in the blood. With further research, this sensor could possibly operate in a greater variety of diagnostic applications than the widely used ELISA.

APPENDIX A

Spectal output of sources used in testing apparatus.

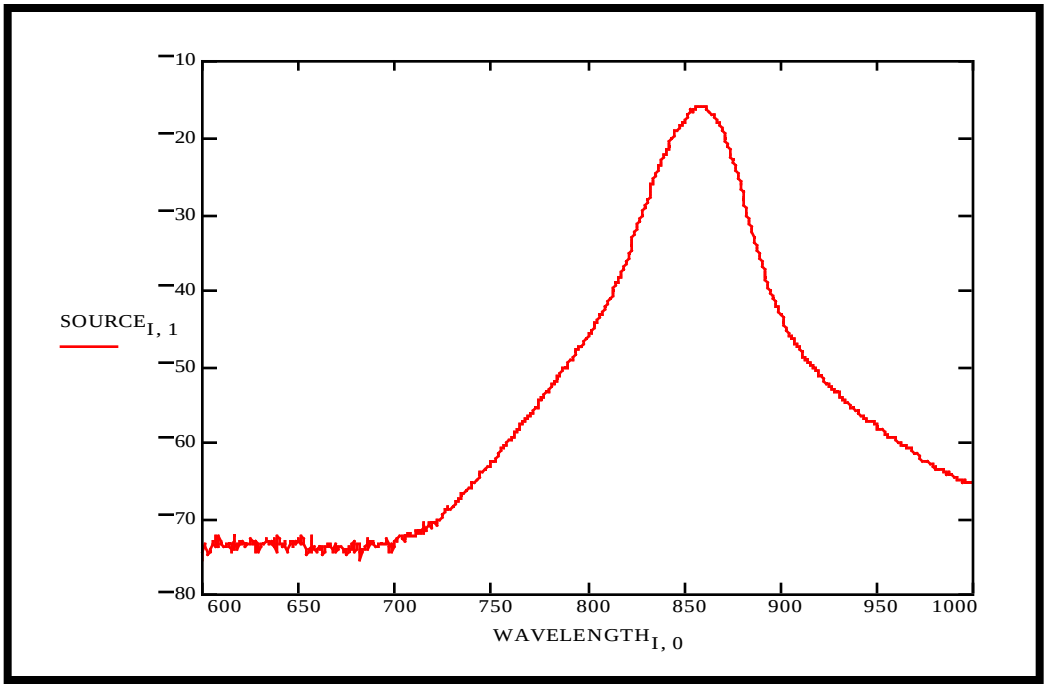

Figure A1: Source 1.

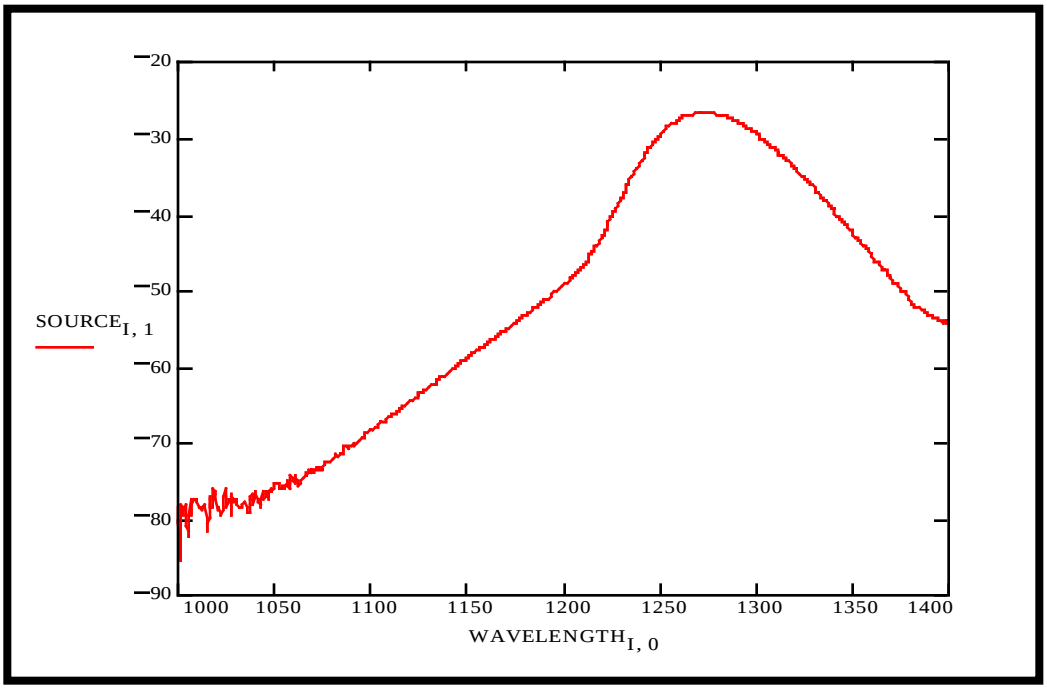

Figure A2: Source 2.

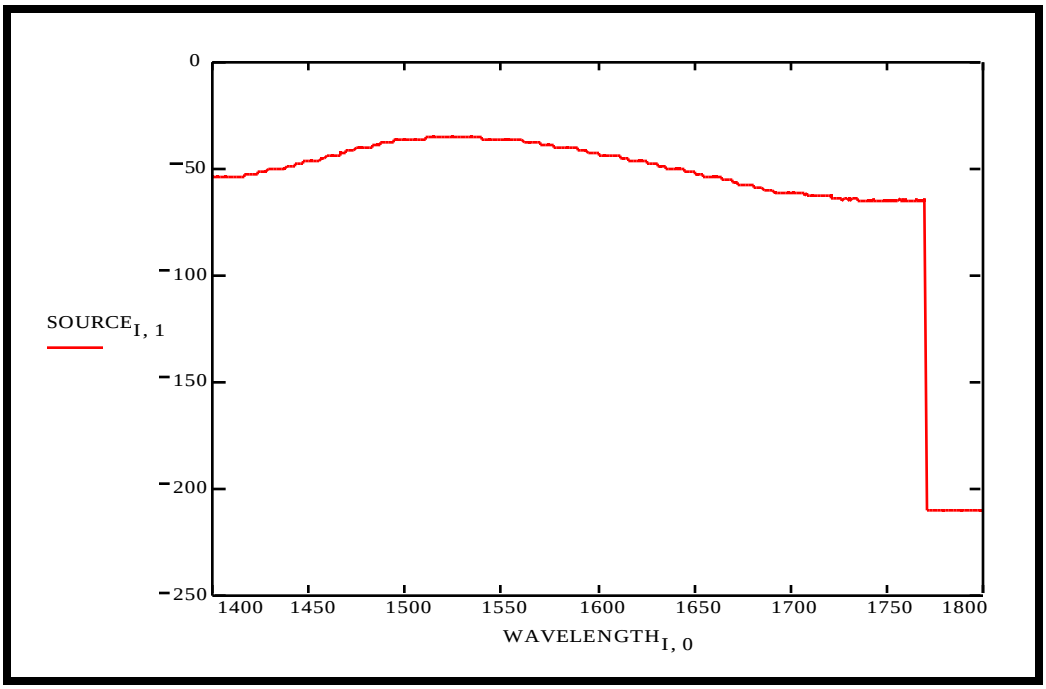

Figure A3: Source 3.

APPENDIX B

Results of antibody-antigen testing for gratings of 40 µm and 160 µm periods.

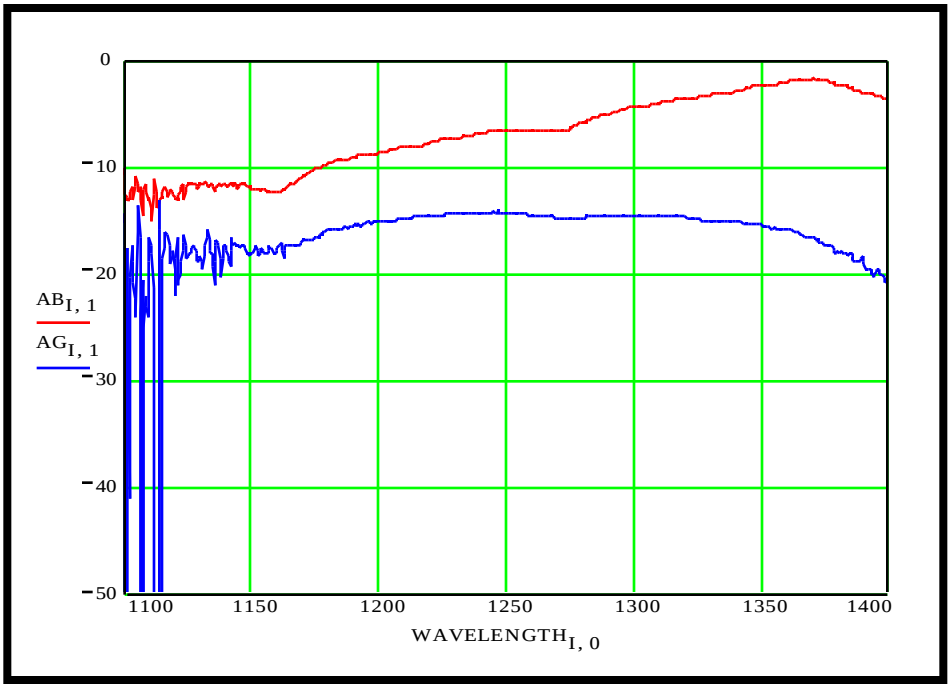

Figure B1: Antibody-antigen test for grating 2/FLX/40 with goat anti-human IgG and human IgG.

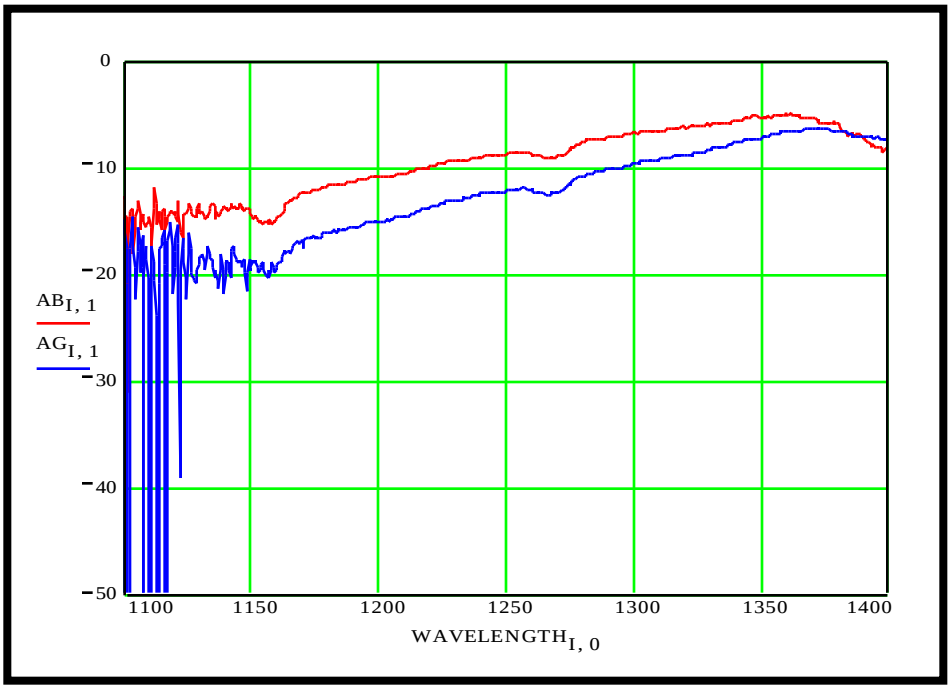

Figure B2: Antibody-antigen test for grating 4/FLX/40 with goat anti-human IgG and horse IgG.

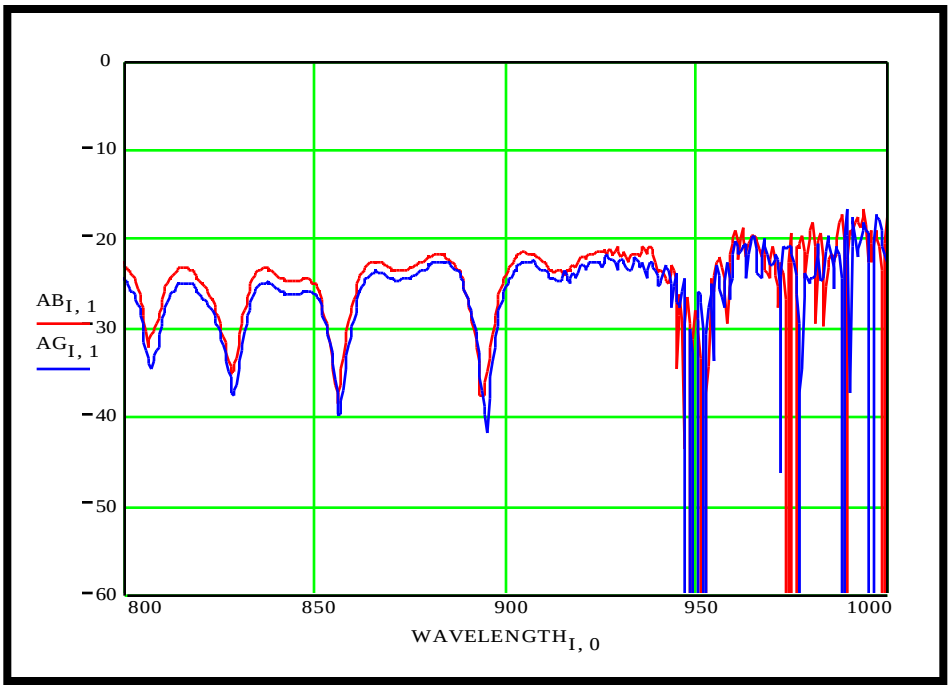

Figure B3: Antibody-antigen test for grating 11/FLX/160 with goat anti-human IgG and human IgG.

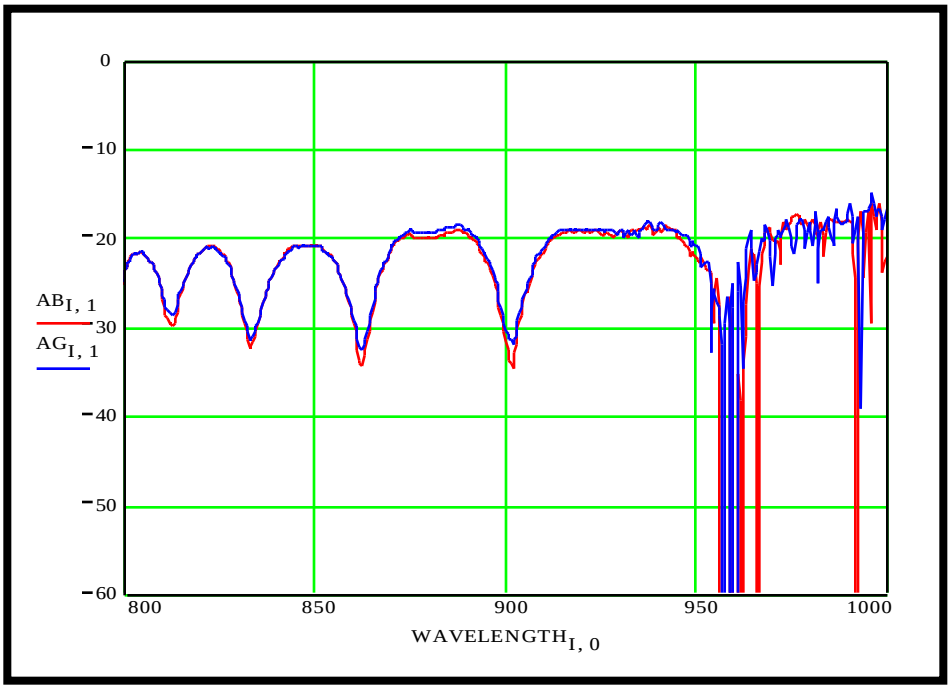

Figure B4: Antibody-antigen test for grating 12/FLX/160 with goat anti-human IgG and human IgG.

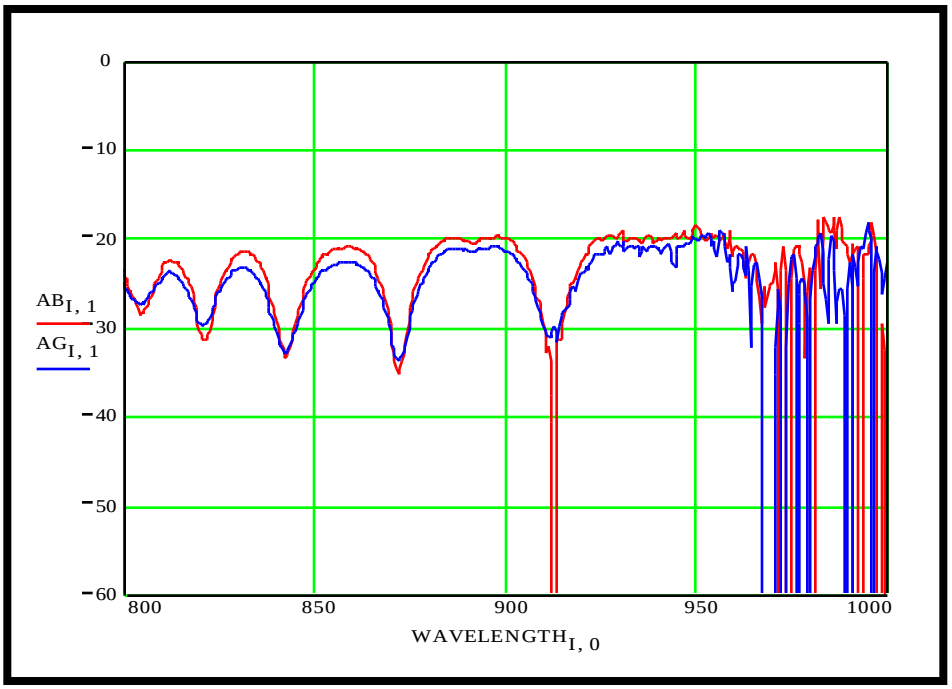

Figure B5: Antibody-antigen test for grating 13/FLX/40 with goat anti-human IgG and horse IgG.

REFERENCES

[1] *Pierce Catalog & Handbook, Life Science & Analytical Research Products.* Pierce Chemical Company, Rockford, IL, 1994.

[2] G. P. Anderson, J. P. Golden, L. K. Cao, D. Wijesuriya, L. C. Shriver-Lake, F. S. Ligler. "Development of an Evanescent Wave Fiber Optic Biosensor." *IEEE Engineering in Medicine and Biology.* June/July 1994, pp. 358 - 363.

[3] E. Lee. *EL1 Laboratory Notebooks.* Fralin Biotechnology Center, Virginia Polytechnic Institute and State University, 1995.

[4] S. K. Bhatia, L. C. Shriver-Lake, K. J. Prior, J. H. Georger, J. M. Calvert, R. Bredehorst, R. S. Ligler. "Use of Thiol-Terminal Silanes and Heterobifunctional Crosslinkers for Immobilization of Antibodies on Silica Surfaces." *AnalyticalBiochemistry.* 178, 1989, pp. 408 - 413.

[5] B. Lu, J. Xie, C. Lu, C. Wu, Y. Wei. "Oriented Immobilization of Fab' Fragments on Silica Surfaces." *Analytical Chemistry.* 67, 1995, pp. 83 - 87.

[6] I. Lundstrom. "Real-time biospecific interaction analysis." *Biosensors & Bioelectronics.* Vol 9, 1994, pp. 725 - 736.

[7] I. Faulkner, W. R. Flavell, J. Davies, R. F. Sunderland, C. S. Nunnerly. "SPR-based Sensors studied by Electron Energy Loss Spectroscopy and Attenuated Total Reflection." *Journal of Electron Spectroscopy and Related Phenomena.* Vol 64/65, 1993, pp. 441 - 450.

[8] S. Lofas, B. Johnsson. "A Novel Hydrogel Matrix on Gold Surfaces in Surface Plasmon Resonance Sensors for Fast and Efficient Covalent Immobilization of Ligands." *Journal of the Chemical Society.* Chemical Communications, 1990, pp. 1526 - 1528.

[9] E. Stenberg, B. Persson, H. Roos, C. Urbaniczky. "Quantitative Determination of Surface Concentration of Protein with Surface Plasmon Resonance Using Radiolabeled Proteins." *Journal of Colloid and Interface Science.* Vol 143, No 2, May 1991, pp. 513 - 526.

[10] A. M. Vengsarkar, J. R. Pedrazzani, J. B. Judkins, P. J. Lemaire, N. S. Bergano, C. R. Davidson. "Long-period fiber-grating-based gain equalizers." *Optics Letters.* Vol 21, No 5, March 1, 1996, pp. 336 - 338.

[11] R. Kashyap. "Photosensitive Optical Fibers: Devices and Applications." *Optical Fiber Technology.* 1, 1994, pp. 17 - 34.

[12] A. M. Vengsarkar, P. J. Lemaire, J. B. Judkins, V. Bhatia, T. Erdogan, J. E. Sipe. "Long-period fiber gratings as band-rejection filters." *Proc. Conference on Optical Fiber Communications.* Post-deadline paper, PD4, 1995.

[13] V. Bhatia. *Properties and Sensing Applications of Long-Period Gratings.* Ph. D. Dissertation. Virginia Polytechnic Institute and State University, 1996.

[14] V. Bhatia, D. K. Campbell, D. Sherr, T. D'Alberto, N. A. Zabaronick, G. A. Ten Eyck, K.

[14] V. Bhatia, D. K. Campbell, D. Sherr, T. D'Alberto, N. A. Zabaronick, G. A. Ten Eyck, K. A. Murphy, R. O. Claus. "Applications of Temperature-Insensitive and Strain-Insensitive Long-Period Gratings." *Optical Engineering.* 1996.

[15] V. Bhatia, D. Campbell, T. D'Alberto, G. Ten Eyck, D. Sherr, K. A. Murphy, and R. O. Claus, "Standard optical fiber long-period gratings with reduced temperature-sensitivity for strain and refractive index sensing." *Proc. Conference on Optical Fiber Communications.* FB1, 1997.

[16] *Instructions: NHS-Ester-Maleimide Heterobifunctional Crosslinkers.* Pierce Chemical Company, Rockford, IL, 1994.

[17] V. Bhatia, T. D'Alberto, K. A. Murphy, and R. O. Claus, "Etched cladding long-period grating refractive index sensors," submitted to *Electronics Letters*, 1996.

[18] *Catalog Handbook of Fine Chemicals.* Aldrich Chemical Company, Inc, Milwaukee, WI, 1994 - 1995.

ACKNOWLEDGEMENTS

I would like to thank Dr. Kent Murphy, Dr. Richard Claus, and Dr. Iannis Besieris for offering advice and support, organizing cooperation with other departments when needed, and serving on my committee. In addition, I thank Dr. Claus for motivating me to begin working at the Fiber & Electro-Optics Research Center, Dr. Murphy for initiating this research effort, and Dr. Besieris for giving additional insight into the field of electromagnetics.

I am very grateful to Dr. Vikram Bhatia for his extensive research into fiber optic gratings and his invaluable willingness to share knowledge. Jonathon Greene, Mark Jones, and Greg Ten Eyck of Fiber & Sensor Technologies (F&S) are owed a special thanks for technical discussions and insight into grating theory. I thank Greg Ten Eyck and Dan Sherr for their direct contributions to this research including grating characterization and grating fabrication assistance. I am also grateful to Dr. Tuan Tran of F&S who offered time, guidance, and enthusiasm in the early stages of this effort.

For sharing their knowledge of biochemistry, assisting in the investigation of chemical coating techniques, and lending the use of their facilities and time, I thank Dr. Elaine Lee and Dr. Tracy Wilkens of the Fralin Institute of Biotechnology. I offer an immense thanks to Ron Earp of the Chemistry Department for time, knowledge, supplies, and support.

I will always be indebted to my family: my brothers, Alfred D'Alberto III and Anthony D'Alberto; my mother, Margaret Butta; my grandparents, Alfred D'Alberto I and Maria D'Alberto; my aunts, Livia Pazourek, Sylvia Boan, and Nancy Zinc; and most especially, my father, Alfred D'Alberto II. Collectively, they stand for strength, perserverence, hard work, love, and knowledge. They have been and always will be role models in my life. A special thanks is given to Dianne D'Alberto for her support and technical assistance. I also thank Tony Butta for his encouragement. Finally, I would like to thank my beloved dog, Topaz D'Alberto, who didn't live to see the conclusion of this work. Her love will always be remembered and cherished.

VITA

Tiffanie Gabrielle D'Alberto was born in Baltimore, Maryland on April 10, 1971 and raised in the town of Finksburg, Maryland. She skipped fifth grade, participated in gifted and talented programs, and received an Accelerated Academic Certificate from Westminster High School.

In 1988, she entered Virginia Polytechnic Institute and State University (VPI&SU) in a pre-veterinary program. She later transferred to the Electrical Engineering Department and completed a three semester cooperative education program at the Food & Drug Administration's Medical Electronics Branch .

Tiffanie's work at the Fiber & Electro-Optics Research Center began in her senior year. In May, 1995, she received a Bachelor of Science at VPI&SU in Electrical Engineering with minors in Mathematics and Chemistry. She finished her master's program at the same university in January, 1997.

Tiffanie's hobbies include pencil drawing, sewing, working on any kind of puzzle, and watching Star Trek.